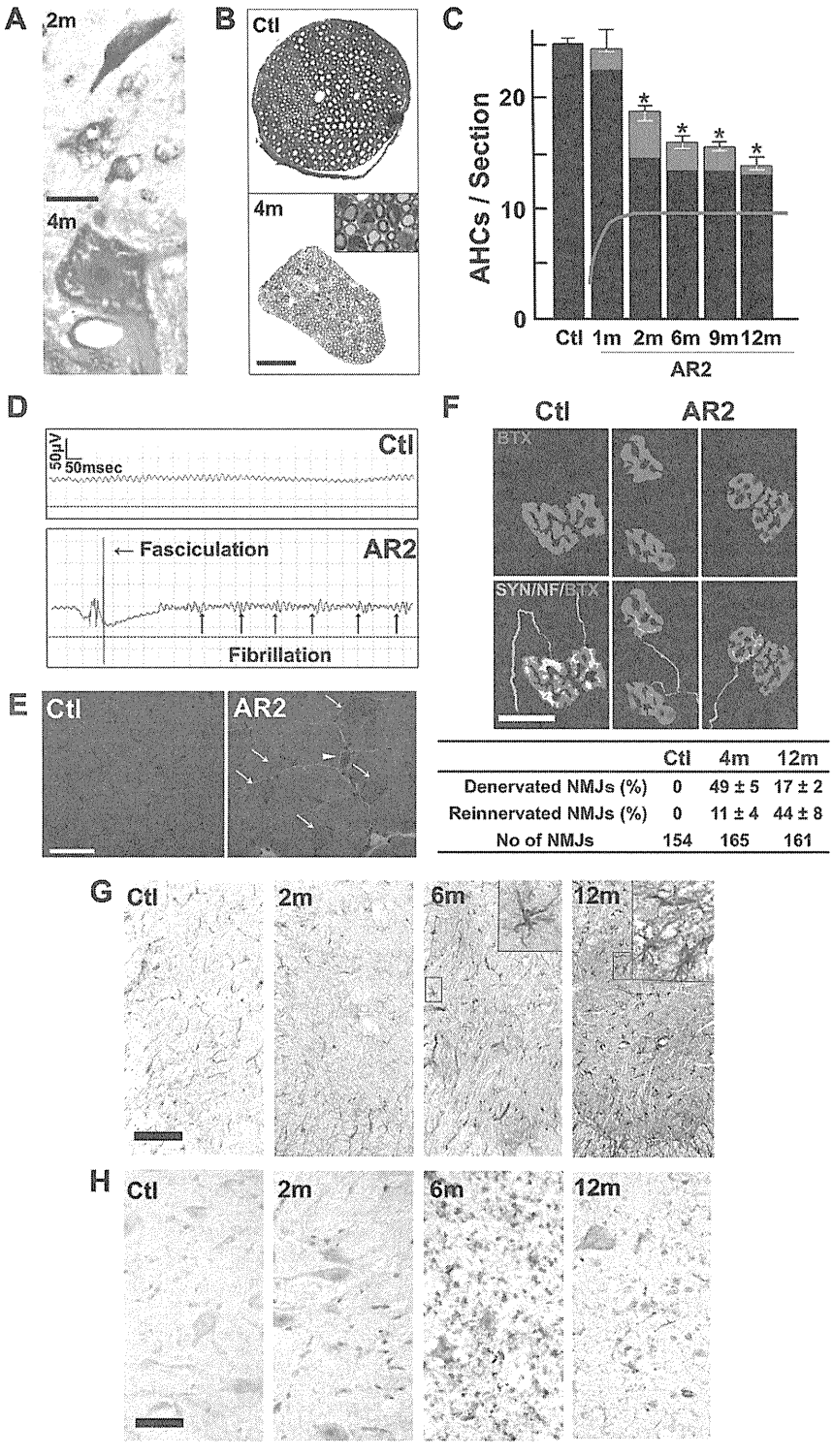


| | Ctl | 4m | 12m |
|---|---|---|---|
| Denervated NMJs (%) | 0 | 49 ± 5 | 17 ± 2 |
| Reinnervated NMJs (%) | 0 | 11 ± 4 | 44 ± 8 |
| No of NMJs | 154 | 165 | 161 |

**Figure 4.** Loss of ADAR2-deficient motor neurons. ***A***, Degenerating AHCs in AR2 mice at 2 months (2m; Nissl staining) and 4 months (4m; toluidine blue staining, 1 $\mu$m section) of age. Scale bar: 2m, 25 $\mu$m; 4m, 12.5 $\mu$m. ***B***, Ventral root (L5) of control (Ctl) and AR2 mice at 4 months of age (4m). Inset, Magnified view of degenerating axons. Scale bar: 100 $\mu$m; inset, 20 $\mu$m. ***C***, Numbers of AHCs showing ADAR2 immunoreactivity (black columns) and lacking this immunoreactivity (gray columns) (mean ± SEM) in AR2 mice at different ages (1m, 2m, 6m, 9m, 12m). In AR2 mice, Cre expression is developmentally regulated (orange line), and ~50% of motor neurons express Cre by 5 weeks of age, with recombination of the *ADAR2* gene in ~10% of AHCs at 1 month of age and 40–45% of AHCs after 2 months of age (orange line). The number of ADAR2-lacking AHCs significantly decreased in AR2 mice after 2 months of age as a result of Cre-dependent knock-out of ADAR2 (*$p < 0.01$, repeated-measures ANOVA). The number of AHCs in the control mice did not change at different ages, and all the AHCs in controls showed ADAR2 immunoreactivity. ***D***, Electrophysiological examination in AR2 mice. Electromyography from an AR2 mouse at 12 months of age showing fibrillations and fasciculations, common findings in ALS indicative of muscle fiber denervation and motor unit degeneration and regeneration.

editing, mean ± SEM: for AR2 mice, 89.7 ± 5.8%, $n = 3$; for control mice, 100%, $n = 3$, $p = 0.0048$) and in the facial nerve nuclei (for AR2 mice, 82.6 ± 9.1%, $n = 3$; for control mice, 99.2 ± 0.2%, $n = 3$, $p = 0.0017$) of AR2 mice at 12 months of age. These results indicate that ADAR2-lacking motor neurons do not always undergo cell death, and some motor neurons, including those in the oculomotor nerve nucleus, are relatively resistant to cell death mediated by deficient ADAR2. Indeed, motor neurons innervating extraocular muscles are much less vulnerable than those innervating bulbar and limb muscles in ALS patients (Lowe and Leigh, 2002).

### GluR-$B^R$ alleles prevent motor neuron death in AR2 mice

To investigate by genetic means the role of RNA editing at the GluR2 Q/R site in the death of motor neurons, we exchanged the endogenous *GluR2* alleles in AR2 mice with GluR-$B^R$ alleles (Kask et al., 1998), which directly encode Q/R site-edited GluR2, thus circumventing the requirement for ADAR2-mediated RNA editing. AR2/GluR-$B^{R/R}$ mice were obtained by *ADAR2*$^{flox/+}$/VAChT–Cre.Fast/GluR-$B^{R/+}$ mice intercrosses to generate *ADAR2*$^{flox/flox}$/VAChT–Cre.Fast/GluR-$B^{R/R}$ (AR2/GluR-$B^{R/R}$) mice (see Materials and Methods).

←

These findings were observed in two other AR2 mice examined but never in control mice (Ctl; $n = 2$). ***E***, Calf muscles from a wild-type mouse (left) and an AR2 mouse (middle and right) at 12 months of age. Characteristics of denervated muscles, including muscle fiber atrophy (white arrow), centrally placed nuclei, and pyknotic nuclear clumps (white arrowhead) are observed in the AR2 mouse. Hematoxylin and eosin. Scale bar, 60 $\mu$m. ***F***, NMJs and distal axons. Quadriceps muscles from a wild-type mouse (Ctl; left) and an AR2 mouse (AR2; middle and right) at 12 months of age are stained with tetramethylrhodamine–bungarotoxin (BTX) (red) and immunostained concomitantly with anti-synaptophysin and neurofilament (SYN/NF) antibodies (green). Endplates (red) were counted as "innervated" if they were merged with axon terminals (merge; yellow). Each endplate is innervated by a thick axon terminal in the Ctl mouse. In AR2 mice, in addition to the normally innervated NMJs, some NMJs were innervated by axons that simultaneously innervate more than one NMJ (reinnervated NMJs; middle), and other NMJs were devoid of axon terminals (denervated NMJs; right). More than 50 NMJs were counted in each animal in the control group and groups of AR2 mice at 4 and 12 months of age ($n = 3$ in each group). Proportions of denervated NMJs and reinnervated NMJs among total NMJs in each group are indicated as mean ± SD (percentage). Scale bar, 25 $\mu$m. ***G***, ***H***, Immunohistochemistry in the anterior horn (C5). There was a time-dependent increase in GFAP immunoreactivity (***G***) and an increase in MAC2 immunoreactivity maximal at 6 months of age (***H***) in the spinal anterior horn of AR2 mice. m, Months of age; inset, activated astroglia. Scale bars: ***G***, 100 $\mu$m; insets and ***H***, 50 $\mu$m.

**Table 1. Density of neurons in motor nerve nuclei and spinal cord**

| Nucleus | Control ($n = 3$) neurons/mm$^3$ | AR2 ($n = 4$) neurons/mm$^3$ |
|---|---|---|
| III | 11,253 ± 1783 | 10,441 ± 632 |
| IV | 15,783 ± 1694 | 16,032 ± 658 |
| VI | 10,117 ± 996 | 10,699 ± 195 |
| Vm | 8809 ± 417 | 8623 ± 246 |
| Vm (>25 μm) | 3603 ± 213 | 2767 ± 175** |
| VII | 1041 ± 124 | 1016 ± 96 |
| VII (>20 μm) | 91.1 ± 32.7 | 67.7 ± 13.1** |
| X | 11,442 ± 1932 | 11,652 ± 2387 |
| XII | 11,800 ± 541 | 9834 ± 1530 |
| XII (>20 μm) | 832.7 ± 92.9 | 677.8 ± 116.2** |
| C5 AH (≤20 μm) | 37,147 ± 326 | 37,941 ± 331 |
| C5 AH (>20 μm) | 25.5 ± 0.9[a] | 13.7 ± 0.7[a,**] |
| L5 AH (>20 μm) | 29.3 ± 0.32[a] | 15.9 ± 0.31[a,**] |
| DH | 476,312 ± 12,623 | 498,816 ± 21,446 |
| VR | 840.0 ± 26.5[b] | 626.3 ± 31.4[b,*] |

Numbers are the neuronal density per cubic millimeter (mean ± SEM) in each nucleus from mice at 12 months of age. For Vm, VII, and XII, neurons with large diameter (>20 or 25 μm) were also counted. AR2, *ADAR2*$^{flox/flox}$/VAChT–Cre.Fast mice; III, nucleus of oculomotor nerve; IV, nucleus of trochlear nerve; VI, nucleus of abducens nerve; Vm, motor nucleus of trigeminal nerve; VII, nucleus of facial nerve; X, dorsal nucleus of the vagus nerve; XII, nucleus of hypoglossal nerve; C5 AH, anterior horn of the fifth cervical cord; L5 AH, anterior horn of the fifth lumbar cord; DH, zona gelatinosa of the spinal cord; VR, ventral roots (L5). *$p < 0.005$; **$p < 0.001$ (ANOVA).

[a]Number of neurons per section.

[b]Number of axons.

AR2/GluR-$B^{R/R}$ mice (AR2rescue, or AR2res, mice) were phenotypically normal and had full motor function until 6 months of age (Fig. 5*A*). The AHCs, including the ~30% AHCs lacking ADAR2 from Cre-mediated recombination, were viable in AR2res mice at 6 months of age, and the total number of AHCs was the same as in age-matched control mice (Fig. 5*A*,*B*). Consistent with a lack of AHC loss, there was no detectable increase in GFAP or MAC2 immunoreactivity in the anterior horns (supplemental Fig. S2*C*, available at www.jneurosci.org as supplemental material). These results demonstrate that it is specifically the failure of GluR2 Q/R site editing by which ADAR2 deficiency induces the slow death of motor neurons (Fig. 5*C*).

## Discussion

We generated the AR2 mouse (Hideyama et al, 2008), a conditional ADAR2 knock-out line, which carries gene-targeted floxed ADAR2 alleles that become functionally ablated by Cre recombinase expressed from a transgene (VAChT–Cre.Fast) in ~50% of motor neurons (Misawa et al., 2003). These displayed progressive motor dysfunctions. The ADAR2-lacking motor neurons expressed only Q/R site-unedited GluR2. Virtually all of the ADAR2-lacking AHCs underwent degeneration, whereas the surviving ADAR2-expressing AHCs remained intact by 12 months of age. The death of ADAR2-lacking AHCs was completely prevented by a point mutation in the endogenous GluR2 alleles of AR2 mice, thus generating Q/R site-edited GluR2 in the absence of ADAR2 (Kask et al., 1998). These findings highlight the crucial role of RNA editing at the GluR2 Q/R site for survival of motor neurons and demonstrate that expression of Q/R site-unedited GluR2 is a cause of slow death of motor neurons. Therefore, it is necessary to investigate the relevance of inefficient GluR2 Q/R site-RNA editing found in the patient's motor neurons to the pathogenesis of sporadic ALS (Kawahara et al., 2004; Kwak and Kawahara, 2005).

Concomitant with the loss of ADAR2-lacking AHCs, proximal and distal axons of AHCs underwent degeneration with resultant neurogenic changes in neuromuscular units. These pathological changes in AHCs and neuromuscular units caused motor dysfunctions in AR2 mice. The prevention of slow neuronal cell death observed in AR2 mice by GluR-$B^R$ alleles expressing Q/R site-edited GluR2 in the absence of ADAR2 (Kask et al., 1998) means that, although ADAR2 edits numerous A-to-I positions in many RNAs expressed in the mammalian brain (Levanon et al., 2004; Li et al., 2009), failure of A-to-I conversions at sites other than the GluR2 Q/R site did not play a role in neuronal cell death (Fig. 5*C*).

When the GluR2 Q/R site is unedited, the $Ca^{2+}$ permeability of the AMPA receptor is greatly increased, and trafficking of the receptor to synaptic membranes is facilitated (Sommer et al., 1991; Burna-

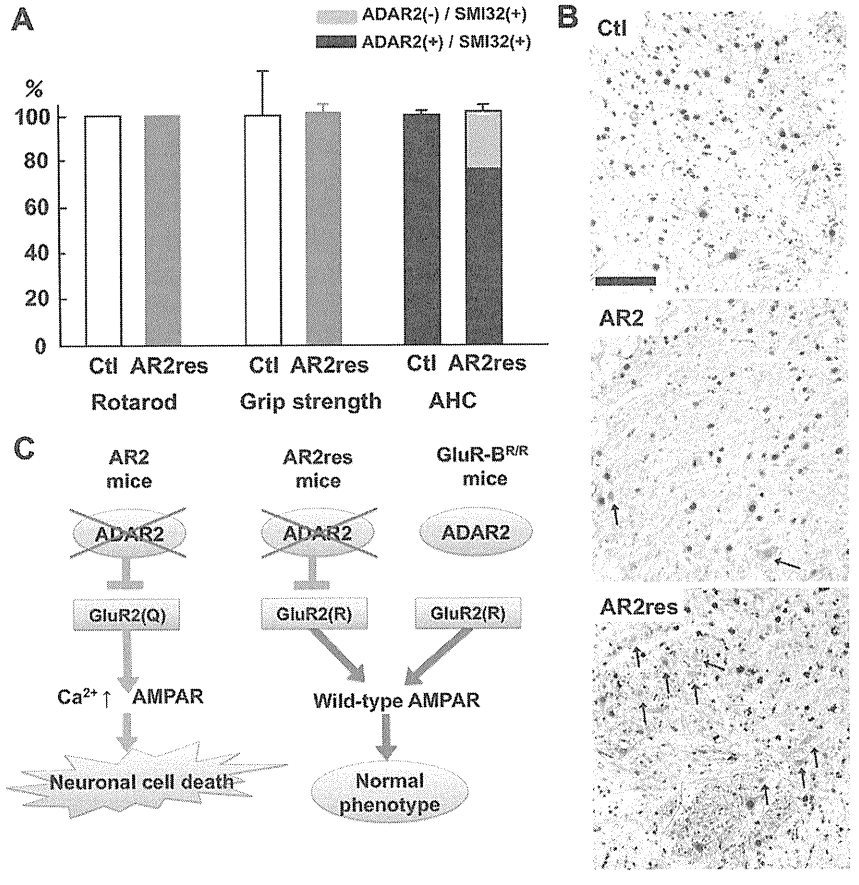


**Figure 5.** Crucial role of GluR2 Q/R site editing in death of ADAR2-deficient motor neurons. ***A***, AR2/GluR-$B^{R/R}$ mice (AR2res) displayed full rotarod score and normal grip strength at 6 months of age compared with control mice (Ctl). The number of total AHCs, of which a considerable proportion was deficient in ADAR2, did not decrease in AR2res mice. ***B***, At 6 months of age, although only a few AHCs lacking ADAR2 immunoreactivity (arrowheads) were observed in AR2 mice, a considerable number of AHCs lacking ADAR2 immunoreactivity was present in AR2res mice. The density of AHCs in AR2res mice was similar to that in the control mice in which all the AHCs were immunoreactive to ADAR2 in their nuclei. Sections were counterstained with hematoxylin. Scale bar, 100 μm. ***C***, Scheme illustrating that lack of ADAR2 induces slow death of motor neurons in AR2 mice but not in AR2res mice that express Q/R site-edited GluR2 in the absence of ADAR2 activity. The exonic Q codon at the Q/R site of GluR2 was substituted by an R codon in the endogenous GluR2 alleles of GluR-$B^{R/R}$ mice.

shev et al., 1992; Greger et al., 2002). This enhances neuronal excitability by increasing the density of $Ca^{2+}$-permeable functional AMPA channels, which is typically observed as fatal epilepsy in mice carrying Q/R site-uneditable GluR-*B* (*GluR2*) alleles (Brusa et al., 1995; Feldmeyer et al., 1999) and in systemic ADAR2-null mice (Higuchi et al., 2000). The results obtained from AR2 mice indicate that motor neurons expressing only Q/R site-unedited GluR2 undergo slow death when the mice live sufficiently long.

Some ADAR2-lacking AHCs die shortly after recombination, whereas others survive for more than 1 year. These observations indicate that, although all the ADAR2-lacking AHCs undergo neuronal death, the ability to compensate for the increased $Ca^{2+}$ overload through the functionally altered AMPA receptor differs among AHCs. It is likely that the increased $Ca^{2+}$ overload might have already led to dysfunction of the ADAR2-lacking AHCs before their death, causing a decline of motor functions at earlier stages. Vulnerability of motor neurons to $Ca^{2+}$-permeable AMPA receptor-mediated toxicity was demonstrated in GluR-B(N) transgenic mice, which additionally to wild-type GluR2 express an engineered GluR2 subunit that features asparagine (N) in place of glutamine (Q) at the Q/R site (Kuner et al., 2005). ADAR2 activity is downregulated in the rat after transient forebrain ischemia, resulting in the selective death of hippocampal CA1 pyramidal cells (Peng et al., 2006).

An intriguing observation in AR2 mice was the selective vulnerability among motor neurons in different cranial nerve nuclei. Neurons in facial and hypoglossal nerve nuclei decreased in number, whereas those in the oculomotor nerve nuclei did not, although the extent of GluR2 Q/R site editing was significantly reduced in all these nuclei. These results indicate that motor neurons in the oculomotor nerve nuclei can survive despite the incomplete nature of GluR2 Q/R site editing. Notably, motor neurons in the nuclei of oculomotor nerves are also much less vulnerable in ALS patients; this has been attributed to differential expression levels of $Ca^{2+}$-binding proteins, particularly parvalbumin, among motor neurons in different cranial nerve nuclei. Expression of parvalbumin is high in oculomotor neurons and low in the facial and spinal motor neurons (Ince et al., 1993). Indeed, overexpression of parvalbumin attenuated kainate-induced $Ca^{2+}$ transients and protected spinal motor neurons from resultant neurotoxicity in parvalbumin transgenic mice (Van Den Bosch et al., 2002). It is likely that neurons with an efficient $Ca^{2+}$-buffering system, such as oculomotor neurons, are resistant to $Ca^{2+}$ overload resulting from $Ca^{2+}$-permeable AMPA receptors.

The present results indicate that the failure of A-to-I conversion at the Q/R site of GluR2 pre-mRNA in motor neurons of sporadic ALS patients (Takuma et al., 1999; Kawahara et al., 2004; Kwak and Kawahara, 2005) is likely attributable to reduced ADAR2 activity. Indeed, the expression level of ADAR2 mRNA was decreased in the spinal cord of patients with sporadic ALS (Kawahara and Kwak, 2005). Molecular abnormalities found in postmortem tissues of patients with neurodegenerative diseases have shown signs of mechanisms underlying the disease and may represent both the neuronal death process and death-protective reactions arising from the protracted nature of the death process. It is therefore necessary to determine whether these molecular abnormalities are the cause or the result of neuronal cell death by developing an appropriate animal model. Although excitotoxicity has long been implicated in the pathogenesis of neurological diseases including ALS (Vosler et al., 2008; Bezprozvanny, 2009), surprisingly little direct evidence indicating excitotoxic neuronal cell death has been demonstrated in patient-derived materials. Here we demonstrate that the molecular abnormality found in motor neurons of patients with sporadic ALS is a direct cause of neuronal death in mice via a mechanism upregulating $Ca^{2+}$-permeable AMPA receptors. In addition, the AR2 mice possess certain characteristics found in ALS, including slow progressive death of motor neurons, neuromuscular unit-dependent motor dysfunction and differential low vulnerability of motor neurons of extraocular muscles. Therefore, this mouse model mimicking patient-derived molecular abnormalities may be useful for research on sporadic ALS.

## References


Akbarian S, Smith MA, Jones EG (1995) Editing for an AMPA receptor subunit RNA in prefrontal cortex and striatum in Alzheimer's disease, Huntington's disease and schizophrenia. Brain Res 699:297–304.

Beleza-Meireles A, Al-Chalabi A (2009) Genetic studies of amyotrophic lateral sclerosis: controversies and perspectives. Amyotroph Lateral Scler 10:1–14.

Bezprozvanny I (2009) Calcium signaling and neurodegenerative diseases. Trends Mol Med 15:89–100.

Brusa R, Zimmermann F, Koh DS, Feldmeyer D, Gass P, Seeburg PH, Sprengel R (1995) Early-onset epilepsy and postnatal lethality associated with an editing-deficient GluR-B allele in mice. Science 270:1677–1680.

Burnashev N, Monyer H, Seeburg PH, Sakmann B (1992) Divalent ion permeability of AMPA receptor channels is dominated by the edited form of a single subunit. Neuron 8:189–198.

Carriedo SG, Yin HZ, Weiss JH (1996) Motor neurons are selectively vulnerable to AMPA/kainate receptor-mediated injury *in vitro*. J Neurosci 16:4069–4079.

Feldmeyer D, Kask K, Brusa R, Kornau HC, Kolhekar R, Rozov A, Burnashev N, Jensen V, Hvalby O, Sprengel R, Seeburg PH (1999) Neurological dysfunctions in mice expressing different levels of the Q/R site-unedited AMPAR subunit GluR-B. Nat Neurosci 2:57–64.

Feng Y, Sansam CL, Singh M, Emeson RB (2006) Altered RNA editing in mice lacking ADAR2 autoregulation. Mol Cell Biol 26:480–488.

Greger IH, Khatri L, Ziff EB (2002) RNA editing at arg607 controls AMPA receptor exit from the endoplasmic reticulum. Neuron 34:759–772.

Greger IH, Khatri L, Kong X, Ziff EB (2003) AMPA receptor tetramerization is mediated by Q/R editing. Neuron 40:763–774.

Hideyama T, Yamashita T, Tsuji S, Misawa H, Takahashi R, Suzuki T, Kwak S (2008) Slow neuronal death of motor neurons in sporadic ALS mouse model by RNA editing enzyme ADAR2 knockout. Soc Abstr Neurosci 34:745.17.

Higuchi M, Maas S, Single FN, Hartner J, Rozov A, Burnashev N, Feldmeyer D, Sprengel R, Seeburg PH (2000) Point mutation in an AMPA receptor gene rescues lethality in mice deficient in the RNA-editing enzyme ADAR2. Nature 406:78–81.

Ince P, Stout N, Shaw P, Slade J, Hunziker W, Heizmann CW, Baimbridge KG (1993) Parvalbumin and calbindin D-28k in the human motor system and in motor neuron disease. Neuropathol Appl Neurobiol 19:291–299.

Kask K, Zamanillo D, Rozov A, Burnashev N, Sprengel R, Seeburg PH (1998) The AMPA receptor subunit GluR-B in its Q/R site-unedited form is not essential for brain development and function. Proc Natl Acad Sci U S A 95:13777–13782.

Kawahara Y, Kwak S (2005) Excitotoxicity and ALS: what is unique about the AMPA receptors expressed on spinal motor neurons? Amyotroph Lateral Scler Other Motor Neuron Disord 6:131–144.

Kawahara Y, Ito K, Sun H, Kanazawa I, Kwak S (2003a) Low editing efficiency of GluR2 mRNA is associated with a low relative abundance of ADAR2 mRNA in white matter of normal human brain. Eur J Neurosci 18:23–33.

Kawahara Y, Kwak S, Sun H, Ito K, Hashida H, Aizawa H, Jeong SY, Kanazawa I (2003b) Human spinal motoneurons express low relative abundance of GluR2 mRNA: an implication for excitotoxicity in ALS. J Neurochem 85:680–689.

Kawahara Y, Ito K, Sun H, Aizawa H, Kanazawa I, Kwak S (2004) Glutamate receptors: RNA editing and death of motor neurons. Nature 427:801.

Kawahara Y, Sun H, Ito K, Hideyama T, Aoki M, Sobue G, Tsuji S, Kwak S (2006) Underediting of GluR2 mRNA, a neuronal death inducing mo-

lecular change in sporadic ALS, does not occur in motor neurons in ALS1 or SBMA. Neurosci Res 54:11–14.

Kuner R, Groom AJ, Bresink I, Kornau HC, Stefovska V, Müller G, Hartmann B, Tschauner K, Waibel S, Ludolph AC, Ikonomidou C, Seeburg PH, Turski L (2005) Late-onset motoneuron disease caused by a functionally modified AMPA receptor subunit. Proc Natl Acad Sci U S A 102: 5826–5831.

Kwak S, Kawahara Y (2005) Deficient RNA editing of GluR2 and neuronal death in amyotropic lateral sclerosis. J Mol Med 83:110–120.

Levanon EY, Eisenberg E, Yelin R, Nemzer S, Hallegger M, Shemesh R, Fligelman ZY, Shoshan A, Pollock SR, Sztybel D, Olshansky M, Rechavi G, Jantsch MF (2004) Systematic identification of abundant A-to-I editing sites in the human transcriptome. Nat Biotechnol 22:1001–1005.

Li JB, Levanon EY, Yoon JK, Aach J, Xie B, Leproust E, Zhang K, Gao Y, Church GM (2009) Genome-wide identification of human RNA editing sites by parallel DNA capturing and sequencing. Science 324:1210–1213.

Lowe JS, Leigh N (2002) Motor neuron disease (amyotrophic lateral sclerosis). In: The Greenfield's neuropathology (Love S, Louis DN, Ellison DW, eds), pp 372–383. Oxford: Oxford UP.

Melcher T, Maas S, Herb A, Sprengel R, Seeburg PH, Higuchi M (1996) A mammalian RNA editing enzyme. Nature 379:460–464.

Misawa H, Nakata K, Toda K, Matsuura J, Oda Y, Inoue H, Tateno M, Takahashi R (2003) VAChT–Cre.Fast and VAChT–Cre.Slow: postnatal expression of Cre recombinase in somatomotor neurons with different onset. Genesis 37:44–50.

Nishimoto Y, Yamashita T, Hideyama T, Tsuji S, Suzuki N, Kwak S (2008) Determination of editors at the novel A-to-I editing positions. Neurosci Res 61:201–206.

Ohmae S, Takemoto-Kimura S, Okamura M, Adachi-Morishima A, Nonaka M, Fuse T, Kida S, Tanji M, Furuyashiki T, Arakawa Y, Narumiya S, Okuno H, Bito H (2006) Molecular identification and characterization of a family of kinases with homology to $Ca^{2+}$/calmodulin-dependent protein kinases I/IV. J Biol Chem 281:20427–20439.

Paschen W, Hedreen JC, Ross CA (1994) RNA editing of the glutamate receptor subunits GluR2 and GluR6 in human brain tissue. J Neurochem 63:1596–1602.

Paxinos G, Franklin KBJ (2001) The mouse brain in stereotaxic coordinates. San Diego: Academic.

Peng PL, Zhong X, Tu W, Soundarapandian MM, Molner P, Zhu D, Lau L, Liu S, Liu F, Lu Y (2006) ADAR2-dependent RNA editing of AMPA receptor subunit GluR2 determines vulnerability of neurons in forebrain ischemia. Neuron 49:719–733.

Rothstein JD, Martin LJ, Kuncl RW (1992) Decreased glutamate transporter by the brain and spinal cord in amyotrophic lateral sclerosis. N Engl J Med 326:1464–1468.

Sansam CL, Wells KS, Emeson RB (2003) Modulation of RNA editing by functional nucleolar sequestration of ADAR2. Proc Natl Acad Sci U S A 100:14018–14023.

Schymick JC, Talbot K, Traynor BJ (2007) Genetics of sporadic amyotrophic lateral sclerosis. Hum Mol Genet 16 [Spec No 2]:R233–R242.

Seeburg PH (2002) A-to-I editing: new and old sites, functions and speculations. Neuron 35:17–20.

Sommer B, Köhler M, Sprengel R, Seeburg PH (1991) RNA editing in brain controls a determinant of ion flow in glutamate-gated channels. Cell 67:11–19.

Suzuki T, Tsuzuki K, Kameyama K, Kwak S (2003) Recent advances in the study of AMPA receptors. Nippon Yakurigaku Zasshi 122:515–526.

Takemoto-Kimura S, Ageta-Ishihara N, Nonaka M, Adachi-Morishima A, Mano T, Okamura M, Fujii H, Fuse T, Hoshino M, Suzuki S, Kojima M, Mishina M, Okuno H, Bito H (2007) Regulation of dendritogenesis via a lipid-raft-associated $Ca^{2+}$/calmodulin-dependent protein kinase CLICK-III/CaMKIgamma. Neuron 54:755–770.

Takuma H, Kwak S, Yoshizawa T, Kanazawa I (1999) Reduction of GluR2 RNA editing, a molecular change that increases calcium influx through AMPA receptors, selective in the spinal ventral gray of patients with amyotrophic lateral sclerosis. Ann Neurol 46:806–815.

Van Damme P, Braeken D, Callewaert G, Robberecht W, Van Den Bosch L (2005) GluR2 deficiency accelerates motor neuron degeneration in a mouse model of amyotrophic lateral sclerosis. J Neuropathol Exp Neurol 64:605–612.

Van Den Bosch L, Schwaller B, Vleminckx V, Meijers B, Stork S, Ruehlicke T, Van Houtte E, Klaassen H, Celio MR, Missiaen L, Robberecht W, Berchtold MW (2002) Protective effect of parvalbumin on excitotoxic motor neuron death. Exp Neurol 174:150–161.

Vosler PS, Brennan CS, Chen J (2008) Calpain-mediated signaling mechanisms in neuronal injury and neurodegeneration. Mol Neurobiol 38: 78–100.

Yang JH, Sklar P, Axel R, Maniatis T (1995) Editing of glutamate receptor subunit B pre-mRNA in vitro by site-specific deamination of adenosine. Nature 374:77–81.

Journal of Neurochemistry JNC

JOURNAL OF NEUROCHEMISTRY | 2010 | 115 | 1150–1160 doi: 10.1111/j.1471-4159.2010.07012.x

# Ammonium chloride and tunicamycin are novel toxins for dopaminergic neurons and induce Parkinson's disease-like phenotypes in medaka fish

Hideaki Matsui,*,† Hidefumi Ito,* Yoshihito Taniguchi,†,‡,[1] Shunichi Takeda†,‡ and Ryosuke Takahashi*,†

*Department of Neurology, Graduate School of Medicine, Kyoto University, Kyoto, Japan

†Core Research for Evolutional Science and Technology (CREST), Japan Science and Technology Agency, Kawaguchi, Japan

‡Department of Radiation Genetics, Graduate School of Medicine, Kyoto University, Kyoto, Japan

**Abstract**

Perturbations in protein folding and degradation are key pathological mechanisms in neurodegenerative diseases, including Parkinson's disease (PD). Recent evidence suggests that mishandling of proteins may play an important role in the pathogenesis of PD. We have utilized medaka fish to monitor the effects of injecting neurotoxins into the CSF space. In this study, ammonium chloride, tunicamycin, and lactacystin were tested for their ability to disturb lysosomal proteolysis, N-glycosylation in the endoplasmic reticulum, and proteasomal degradation, respectively. All of the substances tested induced selective loss of dopaminergic neurons, movement disorders and inclusion bodies. Among them, the features of the inclusion bodies that developed after ammonium chloride injection mimicked those of PD: co-localization of ubiquitin and phosphorylated α-synuclein, as well as the presence of LC3 protein in the inclusion bodies. Our study demonstrated that medaka fish are useful for examining the effects of environmental toxins and lysosome inhibition, and lysosome inhibitors may be factors in the development of PD.

**Keywords:** ammonium chloride, autophagy, lysosome, medaka fish, Parkinson's disease, tunicamycin.

*J. Neurochem.* (2010) **115**, 1150–1160.

Parkinson's disease (PD) is a neurodegenerative disease that is characterized by motor dysfunction, selective loss of dopaminergic and noradrenergic neurons, and proteinaceous inclusion bodies called Lewy bodies. The etiology of PD is largely unknown, but it has been demonstrated that genetic and environmental factors play a role in the development of the disease (Dauer and Przedborski 2003; Warner and Schapira 2003).

Early animal models developed for PD research utilized dopaminergic neuron-specific toxins such as 6-hydroxydopamine and MPTP (Jonsson 1983; Kopin 1987; Bové *et al.* 2005; Smeyne and Jackson-Lewis 2005; Blandini *et al.* 2008). These classical toxins do not seem to produce inclusion bodies (Schober 2004; Bové *et al.* 2005), although there is one exception: continuous MPTP infusion by minipumps can induce inclusion formation (Fornai *et al.* 2005). More recent models have been generated using general toxins such as paraquat, rotenone or proteasome inhibitors (Brooks *et al.* 1999; Betarbet *et al.* 2000; McNaught *et al.* 2004; Uversky 2004). Rotenone and proteasome inhibitors form inclusion bodies containing ubiquitin and α-synuclein that are similar to Lewy bodies in PD brains (Betarbet *et al.* 2000; McNaught *et al.* 2004). These and other undiscovered toxins for dopaminergic neurons may be related to the etiology of human PD.

Previously, we developed MPTP and proteasome inhibitor models in medaka fish that displayed many features of PD (Matsui *et al.* 2009, 2010b). Medaka fish have proven to be practical for environmental toxin exposure studies because of

Received June 2, 2010; revised manuscript received August 25, 2010; accepted September 7, 2010.

Address correspondence and reprint requests to Dr Takahashi, Department of Neurology, Graduate School of Medicine, Kyoto University, 54 Shogoin-Kawahara-cho, Sakyo-ku, Kyoto 606-8507, Japan. E-mail: ryosuket@kuhp.kyoto-u.ac.jp and Dr Takeda, Department of Radiation Genetics, Graduate School of Medicine, Kyoto University, Yoshida-Konoe-cho, Sakyo-ku, Kyoto 606-8501, Japan.
E-mail: stakeda@rg.med.kyoto-u.ac.jp

[1]The present address of Yoshihito Taniguchi is the Department of Preventive Medicine and Public Health, School of Medicine, Keio University, 35 Shinano-cho, Shinjuku-ku, Tokyo 160-8582, Japan.

*Abbreviations used*: ER, endoplasmic reticulum; KDEL, Lys-Asp-Glu-Leu; PD, Parkinson's disease; TH, tyrosine hydroxylase.

their small size and the accessibility of their CNS. Using this model system, we report novel toxins for dopaminergic neurons: a lysosome inhibitor, ammonium chloride, and an N-glycosylation inhibitor, tunicamycin.

## Materials and methods

### Treatment of cells and medaka fish with ammonium chloride, tunicamycin and lactacystin

Ammonium chloride (Wako Pure Chemical, Osaka, Japan), tunicamycin (Nacalai Tesque, Kyoto, Japan) and lactacystin (Kyowa Medex, Tokyo, Japan) were dissolved in 50% dimethylsulfoxide/50% distilled water (v/v). SH-SY5Y cells, from a human dopaminergic cell line, were treated with a vehicle control, 15 mM ammonium chloride, 0.1 μg/mL tunicamycin, or 5 μM lactacystin.

For the treatment of medaka fish, wild-type medaka of the *Kyoto-cab* strain at 10 months post-fertilization were used. Substances were injected into CSF space as previously described (Matsui *et al.* 2010b). Briefly, medaka were anesthetized with chloretone (Tokyo Chemical Industry, Tokyo, Japan). Each fish was moved into an agarose-gel plate with a dent filled with water, then injected with toxins or non-toxic vehicles at a dosage of 0.8 μL/0.1 g body weight. Injections were made using a glass micropipette (GD-1, Narishige, Tokyo, Japan) attached to a Hamilton syringe (Hamilton, Reno, NV, USA). The tip of the glass micropipette was positioned in the CSF space between the hindbrain and the optic tectum. The concentrations of ammonium chloride, tunicamycin, and lactacystin were 100 μg/mL, 100 μg/mL, and 2 mM, respectively.

### Enzyme activity assay

The proteasome activity in the medaka brain was measured as previously described (Matsui *et al.* 2010b). Cathepsin D activity was measured using bovine hemoglobin (Sigma Aldrich, St. Louis, MO, USA) as a substrate. Medaka brain was homogenized and sonicated in 200 μL ice-chilled buffer comprised of 1 mM EDTA and 0.2% (v/v) Tween 20 in phosphate-buffered saline. Homogenates were centrifuged at 14 000 *g* for 5 min at 4°C and the supernatant was used for the subsequent assay. The reaction mixture consisted of 100 μL of 2.5% (w/v) hemoglobin, 50 μL of 0.1 M sodium acetate buffer (pH 4.0) and 25 μL of enzyme extract (containing 20 μg of protein). The mixture was incubated for 16 h at 37°C, then 150 μL of 15% (w/v) trichloroacetic acid was added into the mixture. The assay mixture was centrifuged at 20 000 *g* for 5 min at 20°C. The supernatant was neutralized by adding 8% (v/v) 4 M NaOH and the trichloroacetic acid-soluble peptides in the supernatant were measured by the BCA assay kit (Thermo Fischer, Waltham, MA, USA).

Cathepsin H activity was measured using Arg-MCA (methylcoumarin anilide) (Peptide Institute, Osaka, Japan) as a substrate. Medaka brain was homogenized and sonicated in 200 μL ice-chilled buffer comprised of 1 mM EDTA and 0.2% (v/v) Tween 20 in phosphate-buffered saline. Homogenates were centrifuged at 14 000 *g* for 5 min at 4°C and the supernatant was used for the subsequent assay. The reaction mixture consisted of 20 μM of the substrate, 40 mM sodium acetate buffer (pH 4.0) and 10 μL of enzyme extract (containing 10 μg protein). The mixture was incubated for 2 h at 37°C, and then the released AMC (7-amino-4-methylcoumarin) was detected by fluorescence at 460 nm (emission 355 nm) (Fluoroskan Ascent FL, Thermo Fischer).

### Western blotting and dot blot analysis

Western blotting was conducted as previously described (Matsui *et al.* 2010a). For dot blot analysis, 3 μL of sample buffer solution was dropped onto the nitrocellulose membrane, and then the membrane was dried for 30 min and subjected to the antigen-antibody reaction. Anti-tyrosine hydroxylase (TH) (1 : 1000, mouse monoclonal, Millipore, Billerica, MA, USA), anti-tryptophan hydroxylase antibody (1 : 1000, sheep polyclonal, Abcam, Cambridge, MA, USA), anti-Lys-Asp-Glu-Leu (KDEL) antibody (1 : 1000, mouse monoclonal, Merck, Darmstadt, Germany), anti-ubiquitin antibody (1 : 1000, rabbit polyclonal, Dako, Glostrup, Denmark), anti-β-actin antibody (1 : 5000, mouse monoclonal, Sigma Aldrich), anti-pan synuclein antibody (1 : 1000, rabbit polyclonal, Millipore), anti-phosphorylated α-synuclein antibody (1 : 1000, mouse monoclonal, Wako Pure Chemical) and anti-oligomer antibody (A11, 1 : 1000, rabbit polyclonal, Invitrogen, Carlsbad, CA, USA) were used for the assay.

### Immunohistochemistry and transmission electron microscopy

Immunohistochemistry and transmission electron microscopy were conducted as previously described (Matsui *et al.* 2010b). Anti-phosphorylated α-synuclein antibody (1 : 100, mouse monoclonal, Wako Pure Chemical), anti-pan synuclein antibody (1 : 100, rabbit polyclonal, Millipore), anti-α-synuclein antibody (1 : 100, mouse monoclonal, Invitrogen), anti-LC3 antibody (1 : 100, rabbit polyclonal, MBL, Nagoya, Japan), anti-KDEL antibody (1 : 100, mouse-monoclonal, Merck), anti-ubiquitin antibody (1 : 100 for fluorescence imaging and 1 : 500 for diaminobenzidine (DAB) staining, rabbit polyclonal, Dako) and anti-ubiquitin antibody (1 : 100, mouse monoclonal, Santa Cruz Biotechnology, Santa Cruz, CA, USA) were used for immunohistochemistry.

### *In vitro* kinase reaction of α-synuclein

Four micrograms of recombinant medaka α-synuclein or human α-synuclein was incubated in a buffer containing 25 mM Tris–HCl (pH 7.5), 10 mM $MgCl_2$ and 1 mM ATP with or without 1 unit casein kinase (I or II) (Promega, Madison, WI, USA). The mixture was incubated at 37°C for 1 h. The reaction was stopped by adding sodium dodecyl sulfate sample buffer and boiling at 85°C for 10 min.

### Statistical analysis

Data were expressed as means ± standard errors of the mean (SEM). An ANOVA was used to test results for statistical significance. *Post-hoc* analysis using Bonferroni correction for multiple tests was used. Differences were considered significant when $p < 0.05$.

## Results

### Ammonium chloride, tunicamycin, and lactacystin treatment developed various kinds of inclusions in the human dopaminergic cell line

We first examined whether proteasome inhibition (lactacystin), lysosome inhibition (ammonium chloride), or N-glycosylation inhibition (tunicamycin) could induce

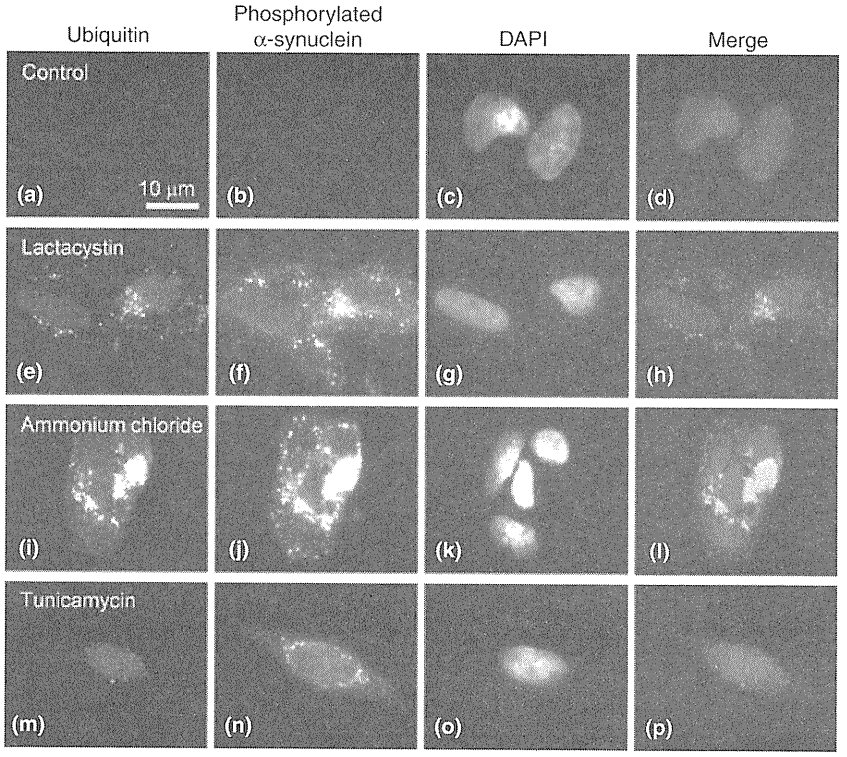


**Fig. 1** Ubiquitin and phosphorylated α-synuclein immunocytochemistry of SH-SY5Y cells treated with vehicle control (a–d), lactacystin (e–h), ammonium chloride (i–l), or tunicamycin (m–p) for 48 h. (a, e, i, m) Ubiquitin (green). (b, f, j, n) Phosphorylated α-synuclein (red). (c, g, k, o) DAPI (blue). (d, h, l, p) Merged image of (a)–(c), (e)–(g), (i)–(k), and (m)–(o), respectively.

inclusion formation in the SH-SY5Y human dopaminergic cell line. We stained the cells with anti-ubiquitin and anti-phosphorylated α-synuclein antibody to see the ubiquitin and/or phosphorylated α-synuclein-positive inclusion formation. Two days after treatment, cells treated with any of the three chemicals developed ubiquitin and/or phosphorylated α-synuclein-positive inclusions (Fig. 1e–p), while the vehicle control did not (Fig. 1a–d). However, the staining pattern differed among the groups. In lactacystin-treated SH-SY5Y cells, many inclusions were only ubiquitin or phosphorylated α-synuclein-positive, although some were double-positive (Fig. 1e–h). In contrast, ammonium chloride treatment resulted in inclusions containing both ubiquitin and phosphorylated α-synuclein (Fig. 1i–l). Tunicamycin treatment induced many phosphorylated α-synuclein-positive inclusions but only a few inclusions contained ubiquitin (Fig. 1m–p). These results were also reproduced when using anti-α-synuclein antibody (Figure S1a–p).

We hypothesized that these inclusion bodies contain different proteins as a result of the toxin that was used. Ammonium chloride inhibits lysosome-autophagosome fusion, which should lead to an accumulation of markers for autophagosomes. On the other hand, tunicamycin induces protein misfolding in the endoplasmic reticulum (ER), which may result in inclusion bodies containing ER proteins. As predicted, ubiquitin-positive inclusion bodies that developed after treatment with ammonium chloride contained LC3, a marker for autophagosomes (Fig. 2A–P). Inclusion bodies expressing this marker did not result from treatment with lactacystin or tunicamycin. Inclusion bodies in tunicamycin-treated cells, and not in lactacystin- or ammonium chloride-treated cells, contained KDEL, a signal sequence for ER chaperones (Fig. 2Q–f).

In summary, ammonium chloride (a lysosome inhibitor), tunicamycin (an N-glycosylation inhibitor), and lactacystin (a proteasome inhibitor) developed inclusion bodies in SH-SY5Y cells with different characteristics according to the toxin used.

### Ammonium chloride and tunicamycin developed ubiquitin-positive inclusions in medaka brain

Next, to examine the effects of ammonium chloride, tunicamycin, or lactacystin in *in vivo* animal models, we administered these substances into medaka CSF using the method previously described (Matsui *et al.* 2010b). At first, we measured lysosome activity (cathepsin D/H activity), ER stress (KDEL expression level), and proteasome activity of medaka brains to check the specific effects of these toxins in medaka whole brain. Cathepsin D/H activity appeared to be up-regulated in ammonium chloride-treated brains, probably because of compensation (Figure S2a and b). KDEL expression was increased in tunicamycin-treated brains, indicating successful induction of ER stress in these brains (Figure S2c). Proteasome activity was decreased in lactacystin-treated brains as previously described (data not shown, Matsui *et al.* 2010b). These data indicate that each chemical induced specific effects in medaka brains *in vivo*.

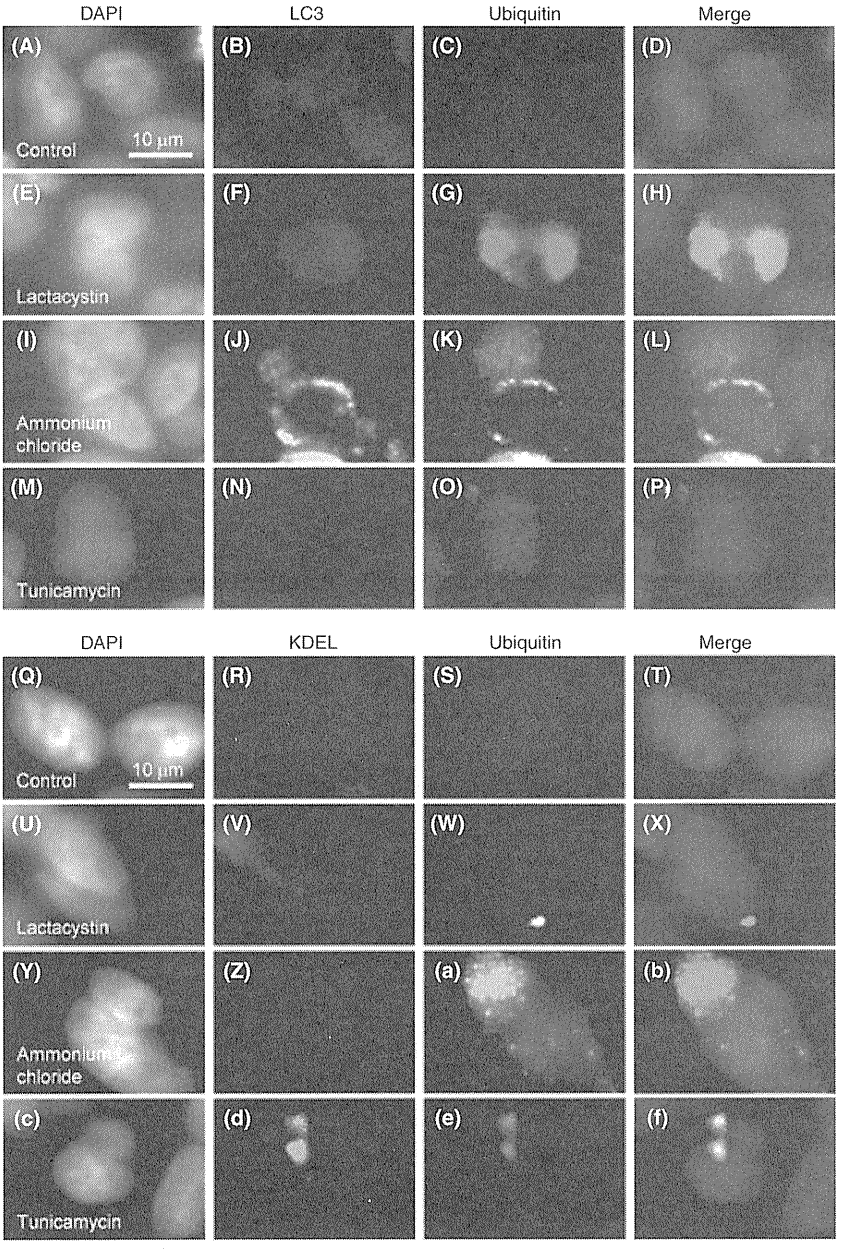


**Fig. 2** Ubiquitin, LC3 and KDEL immunocytochemistry of SH-SY5Y cells treated with vehicle control, ammonium chloride, tunicamycin, or lactacystin for 48 h (A-f). (A–D) Vehicle control. (E–H) Lactacystin. (I–L) Ammonium chloride. (M–P) Tunicamycin. (A, E, I, M) DAPI. (B, F, J, N) LC3. (C, G, K, O) Ubiquitin. (D, H, L, P) Merged image of (A)–(C), (E)–(G), (I)–(K), and (M)–(O), respectively. (Q–T) Vehicle control. (U–X) Lactacystin. (Y–b) Ammonium chloride. (c–f) Tunicamycin. (Q, U, Y, c) DAPI. (R, V, Z, d) KDEL. (S, W, a, e) Ubiquitin. (T, X, b, f) Merged image of (Q)–(S), (U)–(W), (Y)–(a), and (c)–(e), respectively.

Western blotting of medaka brains showed increased amounts of ubiquitin binding proteins following ammonium chloride, tunicamycin, or lactacystin injection compared to the vehicle control (Fig. 3a and b, Matsui *et al.* 2010b). To test whether treatment with ammonium chloride, tunicamycin, or lactacystin resulted in an increase in inclusion bodies in medaka brain, we stained brain sections with an anti-ubiquitin antibody. Three days after administration of ammonium chloride, tunicamycin, or lactacystin, ubiquitin-positive cytoplasmic inclusions were seen in the brain as well as in TH-positive dopaminergic neurons (Fig. 3c–h, Matsui *et al.* 2010b). Treatment with the vehicle did not result in the formation of inclusion bodies (Fig. 3c and f).

Collectively, both ammonium chloride and tunicamycin induced ubiquitin-positive inclusion bodies in medaka brain similar to those induced by the proteasome inhibitors lactacystin and epoxomicin (Matsui *et al.* 2010b).

### Ammonium chloride and tunicamycin induce selective loss of dopaminergic/noradrenergic neurons in medaka fish

We previously described that the proteasome inhibitors lactacystin and epoxomicin developed not only ubiquitin-positive inclusions but also other PD-like phenotypes such as selective loss of dopaminergic/noradrenergic neurons and movement disorder (Matsui *et al.* 2010b). To assess whether ammonium chloride or tunicamycin also cause PD-like phenotypes, we performed western blotting,

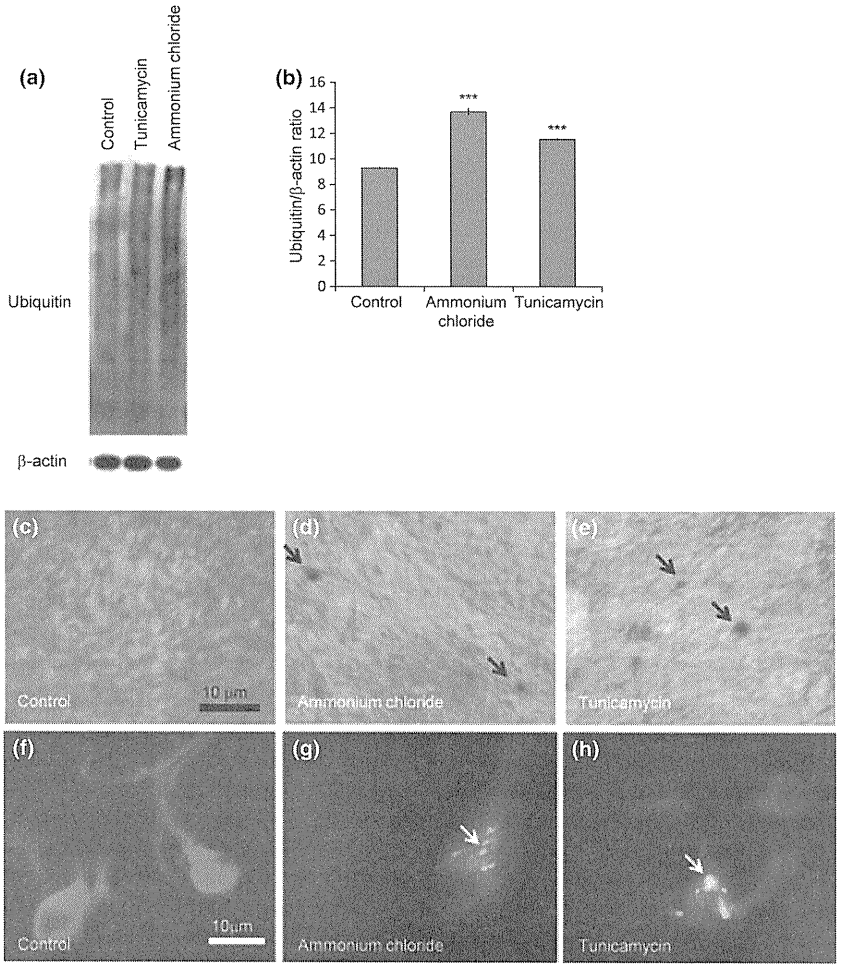


**Fig. 3** Ubiquitin immunohistochemistry and western blotting of medaka brains treated with vehicle control, ammonium chloride, tunicamycin for 3 days. (a) Western blotting of ubiquitin and β-actin of the brains. (b) Densitometric analysis of the western blotting. ***$p < 0.001$ vs. control. (c–e) Anti-ubiquitin antibody staining (DAB staining). (f–h) Anti-ubiquitin (green) and anti-TH (red) antibodies staining (fluorescence imaging). (c, f) Control brain. (d, g) Ammonium chloride-treated brain. (e, h) Tunicamycin-treated brain. Arrows indicate ubiquitin-positive inclusion bodies.

immunohistochemical analysis, HPLC and behavioral assays. Western blotting of medaka whole brain revealed a reduction in TH, a marker of dopaminergic/noradrenergic neurons, in ammonium chloride and tunicamycin-treated medaka fish (Figure S3a and b). Tryptophan hydroxylase, a marker for serotoninergic neurons, did not differ among these groups, indicating selective loss of TH in these brains (Figure S3a). Similar to the case of proteasome inhibitors, ammonium chloride and tunicamycin treatment reduced TH-positive dopaminergic neurons in the middle diencephalon (a possible equivalent of the substantia nigra in mammals) and TH-positive noradrenergic neurons in the medulla oblongata (Fig. 4a–m). Nissl-positive neurons in the optic tectum were not reduced, further indicating selective loss of TH-positive neurons (Fig. 4n). To evaluate whether these substances induced apoptosis, we conducted TdT-mediated dUTP-biotin nick end labeling (TUNEL) assay using the methods previously described (Matsui *et al.* 2010a). In the middle diencephalon of ammonium chloride-treated and tunicamycin-treated medaka brain, TdT-mediated dUTP-biotin nick end labeling (TUNEL) and TH double-labeled cells were observed (Fig. 4o–v), but they were not observed in vehicle-treated cells. These findings indicate that ammonium chloride and tunicamycin treatment indeed induced cell death of TH-positive neurons in the middle diencephalon, at least partly by apoptosis. To measure the amount of catecholamine species, medaka whole brain was subjected to HPLC analysis. Results show a reduction in dopamine and noradrenaline but not in serotonin, providing further evidence of selective loss of dopaminergic/noradrenergic neurons following ammonium chloride and tunicamycin treatment (Figure S4a–c). Finally, we traced and analyzed the swimming behavior of medaka fish using the method previously described (Matsui *et al.* 2010b). The behavioral assay showed a decrease in spontaneous swimming movement in ammonium chloride- and tunicamycin-treated medaka fish (Figure S5a–c).

In summary, ammonium chloride and tunicamycin treatment caused selective loss of dopaminergic/noradrenergic neurons and movement disorder, similar to human PD.

### Ammonium chloride, tunicamycin, and lactacystin showed different kinds of inclusion bodies in the brain of medaka fish

Because Lewy bodies are known to contain not only ubiquitin but also phosphorylated α-synuclein, we stained

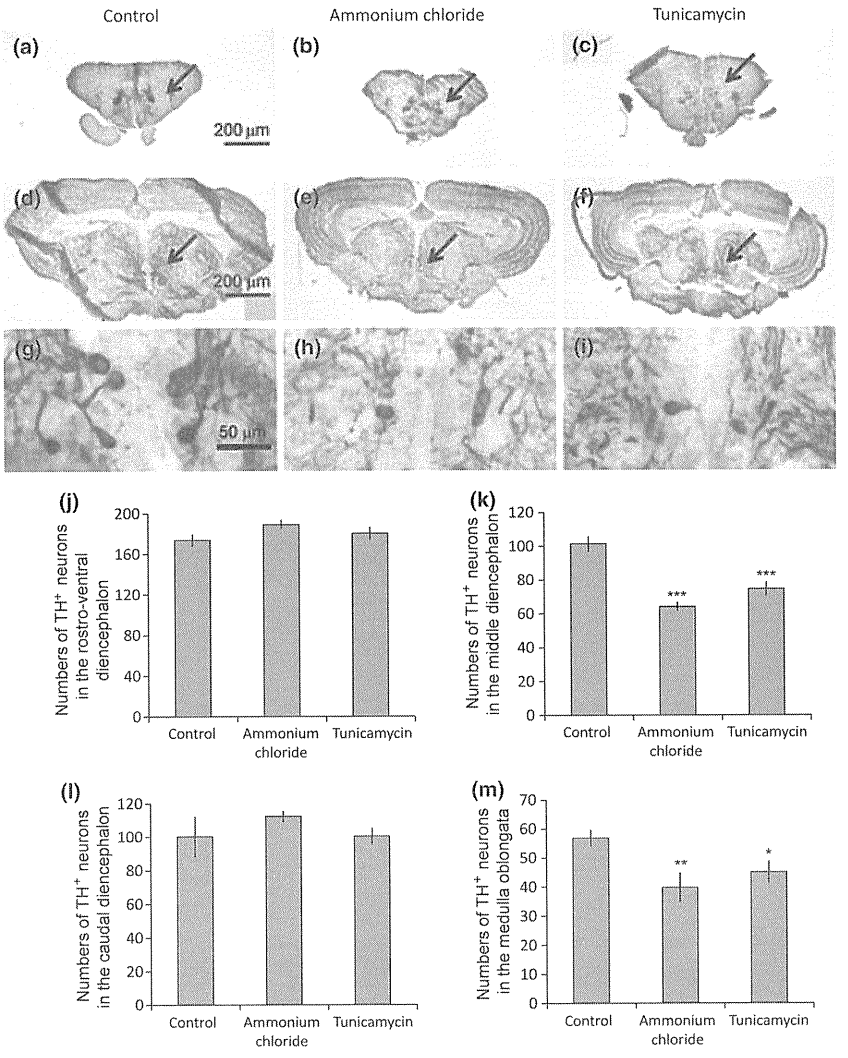


**Fig. 4** Anti-TH antibody and TUNEL staining of vehicle control-, ammonium chloride-, and tunicamycin-treated brain sections. (a–c) TH-positive fibers (arrows) in the forebrain. (d–f) TH-positive neurons (arrows) in the middle diencephalon. (g–i) Enlarged images of (d)–(f), respectively. (a, d, g) Control brains. (b, e, h) Ammonium chloride-treated brains. (c, f, i) Tunicamycin-treated brains. (j–m) Numbers of TH-positive neurons in the rostro-ventral diencephalon (j), middle diencephalon (k), caudal diencephalon (l) and medulla oblongata (m). $^{***}p < 0.001$, $^{**}p < 0.01$, $^{*}p < 0.05$ vs. control ($n = 6$). (n) Number of Nissl-positive neurons in the optic tectum ($n = 6$). (o–r) Ammonium chloride-treated brain. (s–v) Tunicamycin-treated brain. (o, s) DAPI staining. (p, t) Anti-TH antibody staining. (q, u) TUNEL staining. (r, v) Merged image of (o)–(q) and (s)–(u), respectively. Arrows indicate TUNEL-positive TH neurons in the middle diencephalon.

medaka brains with anti-phosphorylated α-synuclein antibody. We first tested whether anti-phosphorylated α-synuclein antibody binds to phosphorylated medaka α-synuclein. Phosphorylated medaka α-synuclein was produced by *in vitro* kinase reaction with recombinant medaka α-synuclein and casein kinase I or II. Dot blot analysis showed that anti-phosphorylated α-synuclein antibody reacted with phosphorylated human and medaka α-synuclein but not with non-phosphorylated human and medaka α-synuclein (Figure S6a).

Next, we performed western blotting of medaka whole brain using this anti-phosphorylated α-synuclein antibody. The result showed an increased amount of high molecular weight bands in tunicamycin- and ammonium chloride-treated fish (Figure S6b). Anti-oligomer specific antibody disclosed increased immunochemical signals in these fish, indicating increased amount of α-synuclein oligomer in tunicamycin- and ammonium chloride-treated fish (Figure S6c). Immunohistochemical analysis showed that ammonium chloride, tunicamycin, and lactacystin treatment increased ubiquitin-positive inclusions while vehicle control did not. Ammonium chloride- and tunicamycin-treated brain also revealed an increased amount of phosphorylated α-synuclein-positive inclusions, but such inclusions were not found in lactacystin- or vehicle-treated groups (Fig. 5a–r). Pre-absorption by medaka phosphorylated α-synuclein diminished the signals of anti-phosphorylated α-synuclein antibody, indicating that this antibody indeed recognized medaka phosphorylated α-synuclein (Fig. 5m–o). Co-localization of ubiquitin and phosphorylated α-synuclein was not seen in vehicle-, tunicamycin-, or lactacystin-treated medaka, but several inclusions in ammonium chloride-treated brain were both ubiquitin- and phosphorylated α-synuclein-positive (Fig. 5a–r). This co-localization was also demonstrated when using anti-α-synuclein and anti-ubiquitin antibodies (Figure S7a–l).

We next examined whether these inclusion bodies contain LC3 or KDEL proteins. Inclusion bodies caused by lactacystin did not contain LC3 or KDEL. However, inclusion bodies in ammonium chloride-treated brains exhibited both anti-ubiquitin and anti-LC3 immunoreactivity.

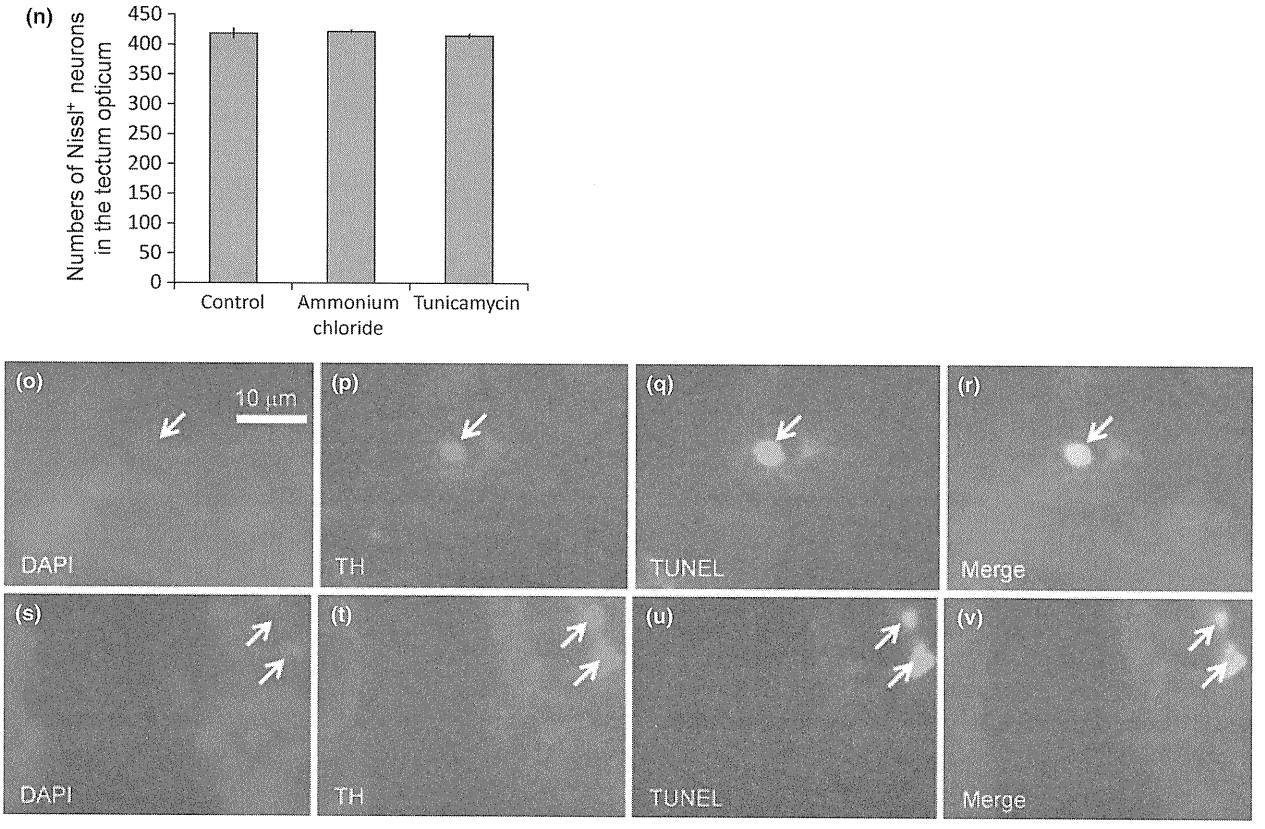


**Fig. 4** *Continued.*

Tunicamycin-treated samples also revealed inclusion bodies that contained both ubiquitin and KDEL (Fig. 6a–r).

Finally, we used transmission electron microscopy to examine the detailed structure of the inclusions. Aggregates with multiple concentric and filamentous structures were observed in the cytoplasm in ammonium chloride-treated medaka brain (Fig. 7a and b). The brain also contained abnormal lysosome-related structures containing whorled membranous material, which were not seen in the vehicle control (Fig. 7c and d). Tunicamycin-treated medaka brain showed abnormal structures containing vacuoles and electron-dense materials (Fig. 7e and f). The brain also contained abnormal lysosome-related structures containing whorled membranous material similar to ammonium chloride samples (Fig. 7g and h).

In conclusion, ammonium chloride, tunicamycin, and lactacystin treatment resulted in the development of various kinds of inclusion bodies, and the characteristics of these inclusion bodies differed depending on the toxins.

## Discussion

In this report, we described that ammonium chloride and tunicamycin caused selective loss of dopaminergic/noradrenergic neurons, movement disorders and inclusion bodies similar to proteasome inhibitor models we previously reported. Although these toxins shared many features of PD, the specific characteristics of the inclusion bodies were dependent on the toxin used.

In Lewy bodies associated with PD, α-synuclein, the protein responsible for familial autosomal dominant PD (Polymeropoulos *et al.* 1997), is phosphorylated and accumulates with ubiquitin (Spillantini *et al.* 1997; Iwatsubo 2003). A recent paper demonstrated that brain samples from α-synuclein transgenic mice and patients with Lewy body disease also showed LC3-positive inclusion bodies (Crews *et al.* 2010). Among the toxins we tested, ammonium chloride seems to better replicate the features typical of Lewy bodies such as co-localization of phosphorylated α-synuclein and ubiquitin, and the presence of LC3 protein in inclusions.

A central issue in the pathogenesis of neurodegeneration is the disturbance of protein folding, aggregation and degradation. There are two major pathways for protein degradation, the ubiquitin-proteasome system and the autophagy–lysosome systems (Ciechanover 2005). Recent evidence suggests an association between PD pathogenesis and autophagy–lysosome systems. Lysosomal clearance has been shown to be disrupted by α-synuclein, which has effects on chaperone-mediated autophagy (Cuervo *et al.*

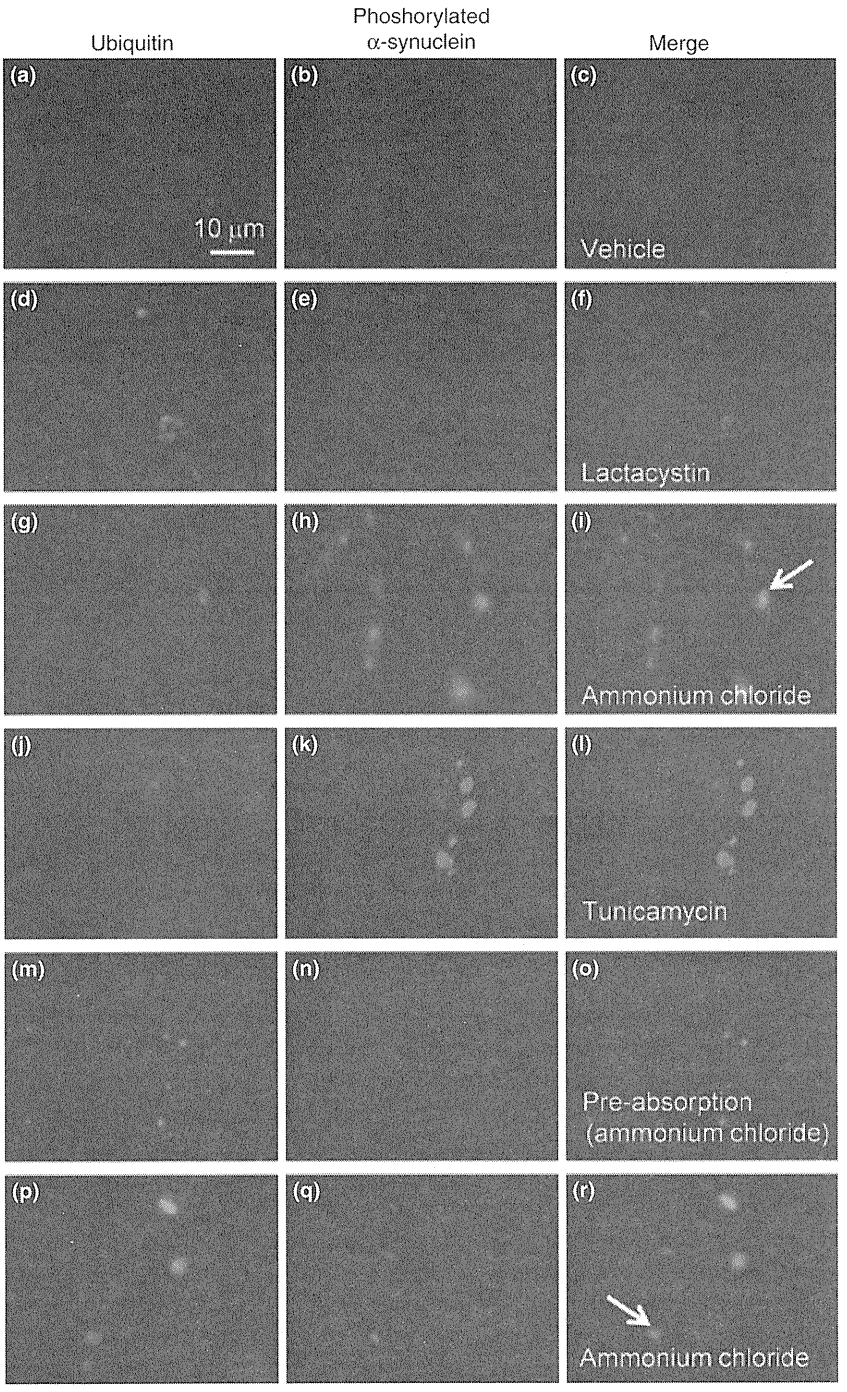


**Fig. 5** Ubiquitin and phosphorylated α-synuclein immunohistochemistry of medaka brains. (a–c) Vehicle control. (d–f) Lactacystin-treated brain. (g–i) Ammonium chloride-treated brain. (j–l) Tunicamycin-treated brain. (m–o) Ammonium chloride-treated brain with anti-phosphorylated α-synuclein antibody pre-absorbed by medaka phosphorylated α-synuclein (10 μg/mL). (p–r) Additional examples of ammonium chloride-treated brain. (a, d, g, j, m, p) Anti-ubiquitin antibody staining. (b, e, h, k, n, q) Anti-phosphorylated α-synuclein antibody staining. (c, f, i, l, o, r) Merged image of (a) and (b), (d) and (e), (g) and (h), (j) and (k), (m) and (n), and (p) and (q), respectively. Arrows indicate ubiquitin and phosphorylated α-synuclein double-positive cells.

2004). Previous studies have shown that lysosome storage diseases such as Gaucher disease and Niemann-Pick disease often develop parkinsonism and α-synuclein accumulation (Tayebi *et al.* 2001; Várkonyi *et al.* 2003; Saito *et al.* 2004). Furthermore, there is now increasing evidence that *parkin* and *PINK1*, genes responsible for autosomal recessive familial PD, play important roles in mitophagy (mitochondria-specific autophagy) and lysosomal clearance of mitochondria (Narendra *et al.* 2008, 2010; Geisler *et al.* 2010; Kawajiri *et al.* 2010; Matsuda *et al.* 2010; Michiorri *et al.* 2010; Vives-Bauza *et al.* 2010). Mouse embryonic fibroblasts deficient in *DJ-1*, another gene responsible for autosomal recessive PD, also showed lysosomal pathology (Krebiehl *et al.* 2010). Furthermore, *Atg7*-deficient mice show neurodegeneration and inclusion bodies similar to Lewy bodies (Komatsu *et al.* 2006). Our results are consistent with prior studies and provide further support for the idea that lysosome inhibition can cause PD.

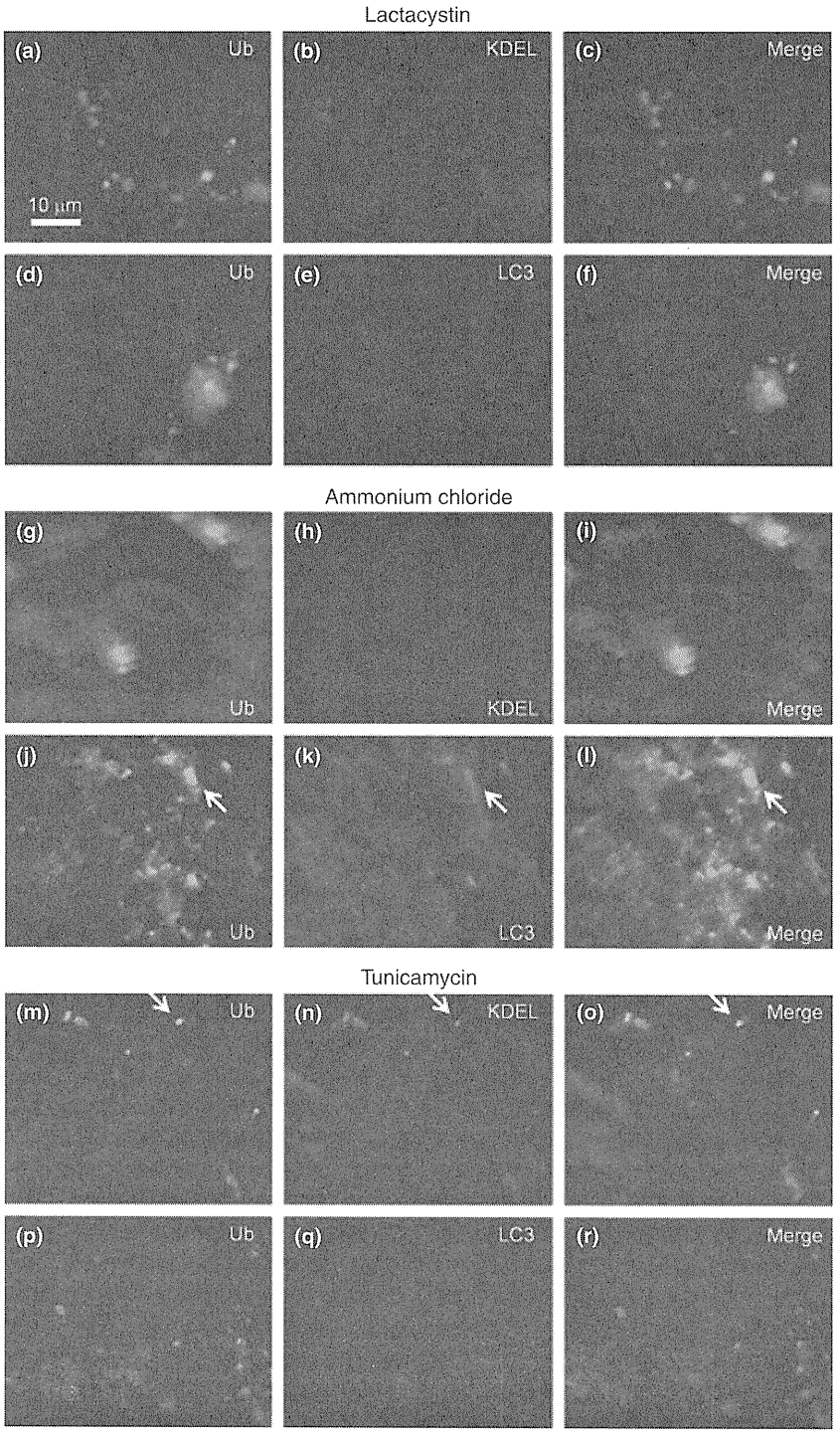


**Fig. 6** Anti-ubiquitin, KDEL, LC3 antibody staining of lactacystin-, ammonium chloride-, and tunicamycin-treated brains. (a–f) Lactacystin-treated brain. (g–l) Ammonium chloride-treated brain. (m–r) Tunicamycin-treated brain. (a, d, g, j, m, p) Anti-ubiquitin antibody staining. (b, h, n) Anti-KDEL staining. (e, k, q) Anti-LC3 staining. (c, f, i, l, o, r) Merged image of (a) and (b), (d) and (e), (g) and (h), (j) and (k), (m) and (n), and (p) and (q), respectively. Arrows indicate an example of ubiquitin/KDEL or ubiquitin/LC3 double-positive cells.

Ammonium chloride has been reported to elevate pH in the lysosome and inhibit phagosome-lysosome fusion (Ohkuma and Poole 1981). This substance can be found naturally in volcanic regions, forming on volcanic rocks near fume-releasing vents. Ammonium chloride is widely used in everyday applications, including cleaning the tip of soldering irons and can also be included in the soldering iron itself. Ammonium chloride is a common ingredient in hair shampoo, textile printing, plywood glue, and some alcoholic drinks. Because ammonium chloride and other substances that inhibit lysosomal function may be related to the etiology of PD, we must examine environmental lysosome inhibitors in general as pathogenic candidates for PD.

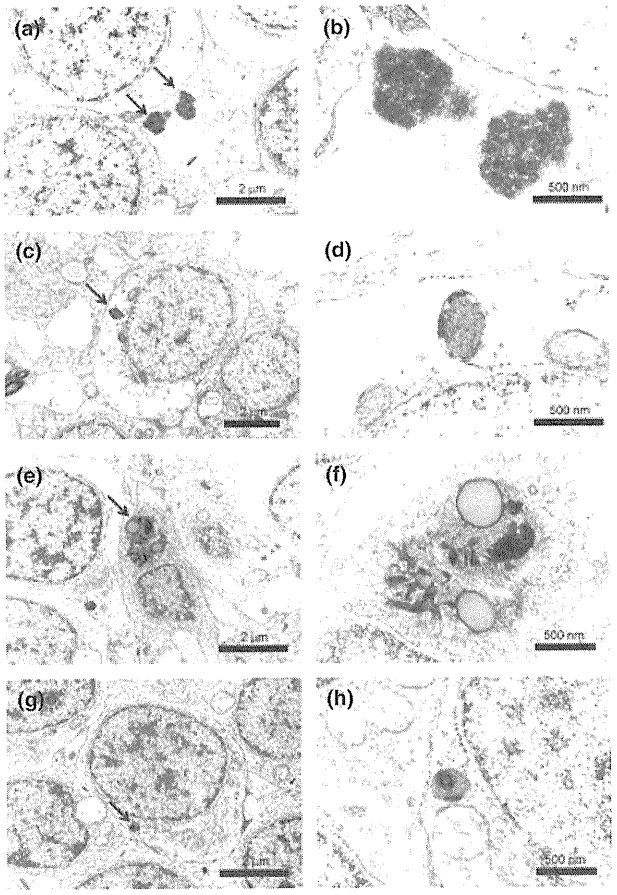


**Fig. 7** Transmission electron microscopic image of ammonium chloride- and tunicamycin-treated brains. (a) Aggregates containing filamentous structures in ammonium chloride-treated brain (arrows). (b) Enlarged image of (a). (c) Abnormal lysosome-related structure containing membranous structures (arrow). (d) Enlarged image of (c). (e) Abnormal structure containing electron dense materials and vacuoles in tunicamycin-treated brain (arrow). (f) Enlarged image of (e). (g) Abnormal lysosome-related structure containing membranous structures (arrow). (h) Enlarged image of (g).

In conclusion, several agents that cause mishandling of proteins can induce PD-like phenotypes. Among the substances we tested, ammonium chloride can replicate Lewy body-like inclusions and may be related to the pathogenesis of PD. Further studies are needed to examine the relationship between lysosomal dysfunction and PD, especially the possibility of lysosome inhibitors as an environmental risk factor.

## Acknowledgement

We wish to thank the Kondoh Differentiation Signaling Project, JST, for permission to use *Kyoto-cab* strain medaka fish. We are grateful to Ai Tanigaki and Dr. Roberto Gavinio, who supported our experiments and English editing, respectively. We are also grateful to Satoshi Fukui for the assistance with our electron microscopy studies.

## Supporting information

Additional Supporting Information may be found in the online version of this article:

**Figure S1.** Ubiquitin and α-synuclein immunocytochemistry of SH-SY5Y cells treated with vehicle control (a–d), lactacystin (e–h), ammonium chloride (i–l), or tunicamycin (m–p) for 48 h.

**Figure S2.** Effects of ammonium chloride, tunicamycin, and lactacystin on whole medaka brain.

**Figure S3.** TH/TPH (tryptophan hydroxylase) western blotting of medaka whole brains treated with vehicle control, ammonium chloride and tunicamycin.

**Figure S4.** HPLC analysis of catecholamine in vehicle control-, ammonium chloride-, and tunicamycin-treated medaka brain ($n = 6$).

**Figure S5.** Spontaneous swimming movement of vehicle control-, ammonium chloride-, and tunicamycin-treated medaka ($n = 9$).

**Figure S6.** Western blotting of anti-phosphorylated α-synuclein antibody in vehicle control-, ammonium chloride-, tunicamycin-, and lactacystin-treated brains.

**Figure S7.** Ubiquitin and synuclein immunohistochemistry of medaka brains.

As a service to our authors and readers, this journal provides supporting information supplied by the authors. Such materials are peer-reviewed and may be re-organized for online delivery, but are not copy-edited or typeset. Technical support issues arising from supporting information (other than missing files) should be addressed to the authors.

## References

Betarbet R., Sherer T. B., MacKenzie G., Garcia-Osuna M., Panov A. V. and Greenamyre J. T. (2000) Chronic systemic pesticide exposure reproduces features of Parkinson's disease. *Nat. Neurosci.* **3**, 1301–1306.

Blandini F., Armentero M. T. and Martignoni E. (2008) The 6-hydroxydopamine model: news from the past. *Parkinsonism Relat. Disord.* **14**(Suppl 2), S124–S129.

Bové J., Prou D., Perier C. and Przedborski S. (2005) Toxin-induced models of Parkinson's disease. *NeuroRx* **2**, 484–494.

Brooks A. I., Chadwick C. A., Gelbard H. A., Cory-Slechta D. A. and Federoff H. J. (1999) Paraquat elicited neurobehavioral syndrome caused by dopaminergic neuron loss. *Brain Res.* **823**, 1–10.

Ciechanover A. (2005) Proteolysis: from the lysosome to ubiquitin and the proteasome. *Nat. Rev. Mol. Cell Biol.* **6**, 79–87.

Crews L., Spencer B., Desplats P., Patrick C., Paulino A., Rockenstein E., Hansen L., Adame A., Galasko D. and Masliah E. (2010) Selective molecular alterations in the autophagy pathway in patients with Lewy body disease and in models of alpha-synucleinopathy. *PLoS ONE* **5**, e9313.

Cuervo A. M., Stefanis L., Fredenburg R., Lansbury P. T. and Sulzer D. (2004) Impaired degradation of mutant alpha-synuclein by chaperone-mediated autophagy. *Science* **305**, 1292–1295.

Dauer W. and Przedborski S. (2003) Parkinson's disease: mechanisms and models. *Neuron* **39**, 889–909.

Fornai F., Schlüter O. M., Lenzi P. *et al.* (2005) Parkinson-like syndrome induced by continuous MPTP infusion: convergent roles of the ubiquitin-proteasome system and alpha-synuclein. *Proc. Natl Acad. Sci. USA* **102**, 3413–3418.

Geisler S., Holmström K. M., Skujat D., Fiesel F. C., Rothfuss O. C., Kahle P. J. and Springer W. (2010) PINK1/Parkin-mediated

mitophagy is dependent on VDAC1 and p62/SQSTM1. *Nat. Cell Biol.* **12**, 119–131.

Iwatsubo T. (2003) Aggregation of alpha-synuclein in the pathogenesis of Parkinson's disease. *J. Neurol.* **250**(Suppl 3), III11–III14.

Jonsson G. (1983) Chemical lesioning techniques: monoamine neurotoxins, in *Handbook of Chemical Neuroanatomy. Methods in Chemical Neuroanatomy* (Björklund A. and Hökfelt T., eds), Edn 1, Vol. 1, pp. 463–507. Elsevier Science Publishers B.V, Amsterdam.

Kawajiri S., Saiki S., Sato S., Sato F., Hatano T., Eguchi H. and Hattori N.. (2010) PINK1 is recruited to mitochondria with parkin and associates with LC3 in mitophagy. *FEBS Lett.* **584**, 1073–1079.

Komatsu M., Waguri S., Chiba T. *et al.*(2006) Loss of autophagy in the central nervous system causes neurodegeneration in mice. *Nature* **441**, 880–884.

Kopin I. J. (1987) MPTP: an industrial chemical and contaminant of illicit narcotics stimulates a new era in research on Parkinson's disease. *Environ. Health Perspect.* **75**, 45–51.

Krebiehl G., Ruckerbauer S., Burbulla L. F. *et al.* (2010) Reduced basal autophagy and impaired mitochondrial dynamics due to loss of Parkinson's disease-associated protein DJ-1. *PLoS ONE* **5**, e9367.

Matsuda N., Sato S., Shiba K. *et al.* (2010) PINK1 stabilized by mitochondrial depolarization recruits Parkin to damaged mitochondria and activates latent Parkin for mitophagy. *J. Cell Biol.* **189**, 211–221.

Matsui H., Taniguchi Y., Inoue H., Uemura K., Takeda S. and Takahashi R. (2009) A chemical neurotoxin, MPTP induces Parkinson's disease like phenotype, movement disorders and persistent loss of dopamine neurons in medaka fish. *Neurosci. Res.* **65**, 263–271.

Matsui H., Taniguchi Y., Inoue H., Kobayashi Y., Sakaki Y., Toyoda A., Uemura K., Kobayashi D., Takeda S. and Takahashi R. (2010a) Loss of PINK1 in medaka fish (Oryzias latipes) causes late-onset decrease in spontaneous movement. *Neurosci. Res.* **66**, 151–161.

Matsui H., Ito H., Taniguchi Y., Inoue H., Takeda S. and Takahashi R. (2010b) Proteasome inhibition in medaka brain induces the features of Parkinson disease. *J. Neurochem.* **115**, 178–187.

McNaught K. S., Perl D. P., Brownell A. L. and Olanow C. W. (2004) Systemic exposure to proteasome inhibitors causes a progressive model of Parkinson's disease. *Ann. Neurol.* **56**, 149–162.

Michiorri S., Gelmetti V., Giarda E. *et al.* (2010) The Parkinson-associated protein PINK1 interacts with Beclin1 and promotes autophagy. *Cell Death Differ.* **17**, 962–974.

Narendra D., Tanaka A., Suen D. F. and Youle R. J. (2008) Parkin is recruited selectively to impaired mitochondria and promotes their autophagy. *J. Cell Biol.* **183**, 795–803.

Narendra D. P., Jin S. M., Tanaka A., Suen D. F., Gautier C. A., Shen J., Cookson M. R. and Youle R. J. (2010) PINK1 is selectively stabilized on impaired mitochondria to activate Parkin. *PLoS Biol.* **8**, e1000298.

Ohkuma S. and Poole B. (1981) Cytoplasmic vacuolation of mouse peritoneal macrophages and the uptake into lysosomes of weakly basic substances. *J. Cell Biol.* **90**, 656–664.

Polymeropoulos M. H., Lavedan C., Leroy E. *et al.* (1997) Mutation in the alpha-synuclein gene identified in families with Parkinson's disease. *Science* **276**, 2045–2047.

Saito Y., Suzuki K., Hulette C. M. and Murayama S. (2004) Aberrant phosphorylation of alpha-synuclein in human Niemann-Pick type C1 disease. *J. Neuropathol. Exp. Neurol.* **63**, 323–328.

Schober A. (2004) Classic toxin-induced animal models of Parkinson's disease: 6-OHDA and MPTP. *Cell Tissue Res.* **318**, 215–224.

Smeyne R. J. and Jackson-Lewis V. (2005) The MPTP model of Parkinson's disease. *Brain Res. Mol. Brain Res.* **134**, 57–66.

Spillantini M. G., Schmidt M. L., Lee V. M., Trojanowski J. Q., Jakes R. and Goedert M. (1997) Alpha-synuclein in Lewy bodies. *Nature* **388**, 839–840.

Tayebi N., Callahan M., Madike V., Stubblefield B. K., Orvisky E., Krasnewich D., Fillano J. J. and Sidransky E. (2001) Gaucher disease and parkinsonism: a phenotypic and genotypic characterization. *Mol. Genet. Metab.* **73**, 313–321.

Uversky V. N. (2004) Neurotoxicant-induced animal models of Parkinson's disease: understanding the role of rotenone, maneb and paraquat in neurodegeneration. *Cell Tissue Res.* **318**, 225–241.

Várkonyi J., Rosenbaum H., Baumann N., MacKenzie J. J., Simon Z., Aharon-Peretz J., Walker J. M., Tayebi N. and Sidransky E. (2003) Gaucher disease associated with parkinsonism: four further case reports. *Am. J. Med. Genet. A* **116**, 348–351.

Vives-Bauza C., Zhou C., Huang Y. *et al.* (2010) PINK1-dependent recruitment of Parkin to mitochondria in mitophagy. *Proc. Natl Acad. Sci. USA* **107**, 378–383.

Warner T. T. and Schapira A. H. (2003) Genetic and environmental factors in the cause of Parkinson's disease. *Ann. Neurol.* **53**(Suppl 3), S16–S23.

 

Journal of Neurochemistry JNC

JOURNAL OF NEUROCHEMISTRY | 2010 | 115 | 178–187 doi: 10.1111/j.1471-4159.2010.06918.x

# Proteasome inhibition in medaka brain induces the features of Parkinson's disease

Hideaki Matsui,*,† Hidefumi Ito,* Yoshihito Taniguchi,†,‡ Haruhisa Inoue,*,†,[1] Shunichi Takeda†,‡ and Ryosuke Takahashi*,†

*Department of Neurology, Kyoto University, Graduate School of Medicine, Kyoto, Japan

†Core Research for Evolutional Science and Technology (CREST), Japan Science and Technology Agency, Kawaguchi, Japan

‡Department of Radiation Genetics, Kyoto University, Graduate School of Medicine, Kyoto, Japan

**Abstract**

Recent findings suggest that a defect in the ubiquitin-proteasome system plays an important role in the pathogenesis of Parkinson's disease (PD). A previous report (McNaught *et al.* 2004) demonstrated that rats systemically injected with proteasome inhibitors exhibited PD-like clinical symptoms and pathology. However, because these findings have not been consistently replicated, this model is not commonly used to study PD. We used medaka fish to test the effect of systemic administration of proteasome inhibitors because of the high level of accessibility of the cerebrospinal fluid in fish. We injected lactacystin or epoxomicin into the CSF of medaka. With proteasome inhibition in the medaka brain, selective dopaminergic and noradrenergic cell loss was observed. Furthermore, treated fish exhibited reduced spontaneous movement. Treatment with proteasome inhibitors also induced the formation of inclusion bodies resembling Lewy bodies, which are characteristic of PD. Treatment with 6-OHDA also induced dopaminergic cell loss but did not produce inclusion bodies. These findings in medaka are consistent with previous results reporting that non-selective proteasome inhibition replicates the cardinal features of PD: locomotor dysfunction, selective dopaminergic cell loss, and inclusion body formation.

**Keywords:** dopamine, hydroxylase, medaka (*Oryzias latipes*), Parkinson's disease, proteasome inhibitor, tyrosine inclusion body.

*J. Neurochem.* (2010) **115**, 178–187.

Parkinson's disease (PD) is characterized by the degeneration of dopaminergic and noradrenergic neurons in neuronal populations located primarily in the substantia nigra pars compacta and the locus coeruleus. Another symptom of PD is the presence of abnormal protein-rich structures known as Lewy bodies and pale bodies in the cytoplasm of neurons in the brainstem or cerebral cortex. Several lines of evidence show that defects in the ubiquitin-proteasome system may play an important role in the pathology of PD (Dawson and Dawson 2003). Mutations in the components of the ubiquitin-proteasome system such as parkin and ubiquitin C-terminal hydrolase L1 are responsible for a subgroup of familial PD (Kitada *et al.* 1998; Leroy *et al.* 1998). Impairment of the ubiquitin-proteasome system has also been implicated in idiopathic PD. For example, a decrement in proteasome activity or a decrease in subunits of the 20S proteasome and the PA700/19S complex was detected in the substantia nigra of PD patients (Tofaris *et al.* 2003; McNaught *et al.* 2006b; Cook and Petrucelli 2009).

Previously, it was reported that systemic exposure to proteasome inhibitors induced dopaminergic neuronal death and the formation of inclusion bodies similar to Lewy bodies (McNaught *et al.* 2004). Although this report widely attracted attention and some groups replicated the original results (Nair *et al.* 2006; Schapira *et al.* 2006; Zeng *et al.*

Received February 25, 2010; revised manuscript received July 9, 2010; accepted July 12, 2010.

Address correspondence and reprint requests to Dr Takahashi, Department of Neurology, Kyoto University, Graduate School of Medicine, 54 Shogoin-Kawahara-cho, Sakyo-ku, Kyoto 606-8507, Japan. E-mail: ryosuket@kuhp.kyoto-u.ac.jp Dr Takeda, Department of Radiation Genetics, Kyoto University, Graduate School of Medicine, Yoshida-Konoe-cho, Sakyo-ku, Kyoto 606-8501, Japan.
E-mail: stakeda@rg.med.kyoto-u.ac.jp

[1]Present address: Center for iPS Cell Research and Application, Institute for Integrated Cell-Material Sciences, Kyoto University 53 Shogoin-Kawahara-cho, Sakyo-ku, Kyoto 606-8507, Japan

*Abbreviations used*: 6-OHDA, 6-hydroxydopamine; PBS, phosphate-buffered saline; PD, Parkinson's disease; TH, tyrosine hydroxylase.

2006), the findings have not been consistently reproduced (Bové *et al.* 2006; Kordower *et al.* 2006; Manning-Boğ *et al.* 2006). The reason for this is unknown, but the authors of the original paper proposed several possibilities, including variation in the brain bioavailability of the toxin (McNaught and Olanow 2006a). To date, the proteasome inhibitors model of PD is not widely accepted as a useful model system for the study of PD (Beal and Lang 2006).

We previously generated genetic and toxin-induced models of PD using a small laboratory fish, medaka (*Oryzias latipes*) (Matsui *et al.* 2009, 2010). In this study, we report a method for the administration of various drugs and toxins into the CSF of medaka. Although we administered proteasome inhibitors and 6-hydroxydopamine (6-OHDA) non-selectively into medaka CSF using this new method, a selective loss of dopaminergic and noradrenergic neurons was induced. Inclusion bodies were observed 3 days after the administration of proteasome inhibitors. This medaka model replicates key features of PD: locomotor dysfunction, inclusion body formation and selective loss of dopamine and noradrenaline neurons.

## Materials and methods

### Proteasome inhibitors and 6-OHDA treatment

Wild-type medaka of the *Kyoto-cab* strain was used for this study. Medaka at 10 months post-fertilization were anesthetized with chloretone at a dosage of 0.35 μg/mL (Tokyo Chemical Industry, Tokyo, Japan). After sufficient anesthesia, each fish was moved into an agarose-gel plate with a dent filled with water (Fig. 1a). Each fish was gently grasped at the belly with the examiner's fingers and injected with toxins or non-toxic vehicles at a dosage of 0.8 μL/0.1 g body weight. The concentrations of toxins were as follows: 2 mM for lactacystin, 10 mM for 6-OHDA and 0.2 mM for epoxomicin. The vehicle for lactacystin and 6-OHDA is water and that for epoxomicin is dimethylsulfoxide. The mean volume (standard error) of injection is 1.52 (0.0045), 1.52 (0.0044), 1.52 (0.0045) μL for vehicle (water), lactacystin and 6-OHDA respectively, and 1.52 (0.0044), 1.52 (0.0045) μL for vehicle (dimethylsulfoxide) and epoxomicin respectively. Injections were made manually (about 1 s/injection) using a glass micropipette (GD-1; Narishige, Tokyo, Japan) attached to a Hamilton syringe (Hamilton, Reno, NV). The tip of the glass micropipette was positioned in the CSF space between the hindbrain and the optic tectum (Fig. 1b). The injection procedures can be seen in the Movie S1.

### Proteasome activity assay

Each brain was homogenized in 200 μL ice-chilled buffer containing 20 mM Tris–HCl pH7.6, 1 mM EDTA, 1 mM dithiothreitol and 0.1% NP40. Homogenates were centrifuged at 14 000 *g* for 5 min at 4°C. The supernatants were used for determination of proteasome activity. Fifty micrograms of protein in 200 μL buffer was incubated with 10 μM Z-Leu-Leu-Glu-AMC (amido-methylcoumarin; Sigma Aldrich, St Louis, MO, USA) for 60 min at 37°C. For the negative control, we added 20 μM epoxomicin in the reaction buffer using vehicle-treated brains. The released AMC was detected at 1 min intervals by fluorescence at 460 nm (emission 355 nm) (Fluoroskan Ascent FL; Thermo Fischer, Waltham, MA, USA).

### Western blotting

Brains were homogenized in RIPA buffer (25 mM Tris–HCl pH 7.6, 150 mM NaCl, 1% NP40, 1% sodium deoxycholate, 0.1% sodium dodecyl sulfate) with protease inhibitors and processed for sodium dodecyl sulfate–polyacrylamide gel electrophoresis. Immunoreactive bands were detected with ECL reagent or ECL plus reagent (GE Healthcare Life Sciences, Buckinghamshire, UK) and the chemiluminescent signal was visualized by exposing the membrane to Fuji RX-U X-ray film (Fuji Film, Tokyo, Japan). Films were scanned and densitometric analysis of blots was performed using ImageJ software (National Institutes of Health; http://rsbweb.nih.gov/ij/). The background intensity of the film was subtracted from the band intensity. A monoclonal antibody against tyrosine hydroxylase (TH) (1 : 1000, mouse monoclonal; Millipore, Billerica, MA, USA) and an anti-tryptophan hydroxylase antibody (1 : 1000, sheep polyclonal; Abcam, Cambridge, MA, USA) were used for the western blotting analysis of TH and tryptophan hydroxylase, respectively. For the detection of ubiquitin, an anti-ubiquitin antibody (1 : 1000, rabbit polyclonal; Dako, Glostrup, Denmark) was used. An anti-β-actin antibody (1 : 5000, mouse monoclonal, AC-15; Sigma-Aldrich, St Louis, MO, USA) was used for the loading control.

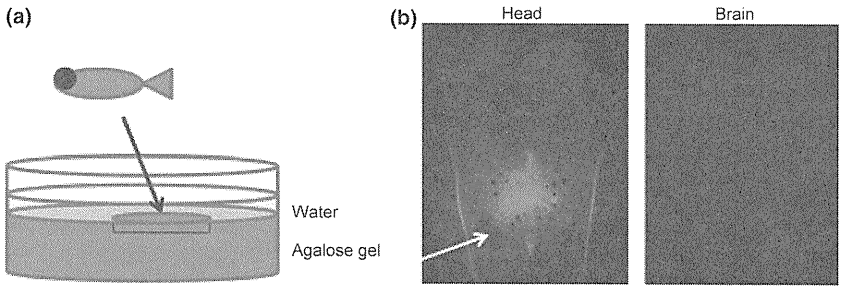


**Fig. 1** Method of injection. (a) Simple illustration of the agarose bed for injection. The dent made it easy to hold the fish stationary. (b) Injected dye in the cerebrospinal fluid space. Images were taken by BIOREVO, BZ-9000 microscope (Keyence, Osaka, Japan). White arrow indicates the route for injection needle. The images were taken from above, soon after the injection of Alexa Fluor 546 (Invitrogen, Carlsbad, CA, USA). The left image is the photograph of the whole head and the right is that of the brain (after removal of the skull and other adjacent structures).

 

### Immunohistochemistry

Immunohistochemistry was performed as previously described with minor modifications (Matsui *et al.* 2009, 2010). Each brain was sectioned at a thickness of 20 μm and sections were incubated with mouse anti-TH antibody (1 : 500, mouse monoclonal; Millipore) for 1 h. Immunoperoxidase detection was carried out using a Vector Elite ABC kit with 3,3′-diaminobenzidine (Vector Laboratories, Burlingame, CA, USA). Densitometric analysis of the striatum TH-positive fibers was performed by Photoshop software (Adobe, San Jose, CA, USA). Several sections were then counter-stained for Nissl substance. For staining of ubiquitin and synuclein, each brain was sectioned at 10 μm and an anti-ubiquitin antibody (1 : 100 for fluorescence, 1 : 500 for 3,3′-diaminobenzidine staining, rabbit polyclonal; Dako) and an anti-synuclein antibody (1 : 100, rabbit polyclonal, AB5464; Millipore) were used, respectively.

To determine the numbers of Nissl-stained cells, we selected the central section from the group of sections containing the middle diencephalic TH-positive cell cluster (when the section number was even, we chose the rostral section). We counted Nissl-stained cells in the optic tectum 300–400 μm lateral from the midline.

The staining specificity was assessed by replacing the primary antibodies with the appropriate amount of phosphate-buffered saline (PBS) solution containing 2% bovine serum albumin or by pre-incubating the primary antibodies with an excess of their respective antigen. No reaction-product deposits were seen in the sections thus treated.

### Transmission electron microscopy

For electron microscopic analysis, medaka brains were fixed overnight in 2% glutaraldehyde with phosphate buffer. After rinsing in 0.1 M PBS with 0.1 M sucrose, samples were post-fixed in 1% osmium tetroxide ($OsO_4$) with 0.1 M PBS and 0.1 M sucrose for 1.5 h. Samples were rinsed, dehydrated in an ethanol series, and embedded in Epon. The 80-nm thin sections were cut on an ultramicrotome. Sections were stained with uranyl acetate and lead citrate.

### Behavioral analysis

Behavioral analysis was performed as previously described with slight modification (Matsui *et al.* 2009, 2010). Image acquisition began 5 min after the medaka was placed in a new water tank. Data were collected continuously for the subsequent 5 min.

### Statistical analysis

Data were expressed as mean ± standard errors of the mean (SEM). An analysis of variance (ANOVA) was used to test results for statistical significance. *Post hoc* analysis using Bonferroni correction for multiple tests was used. Differences were considered significant when $p < 0.05$.

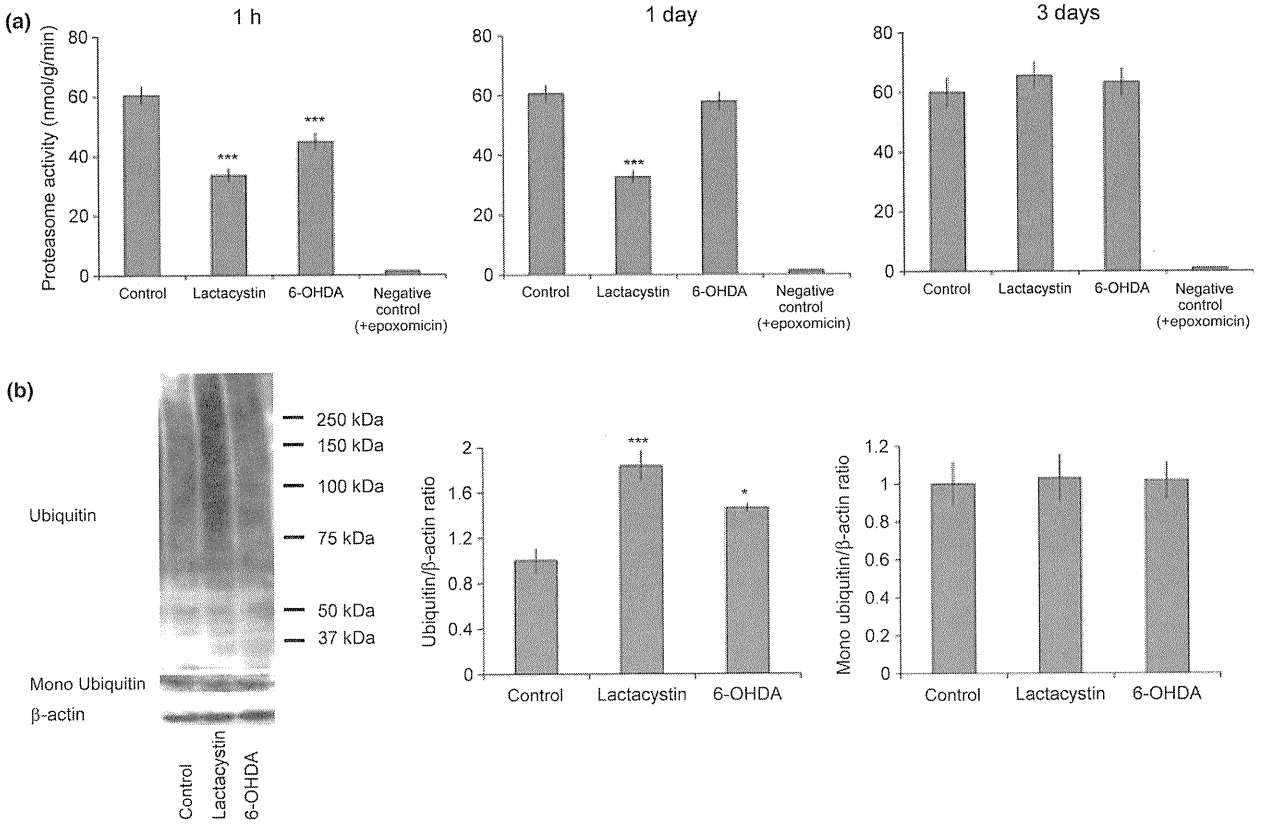


**Fig. 2** Proteasome activity and the amount of ubiquitinated proteins of vehicle-, lactacystin- and 6-OHDA-treated medaka brain. (a) The upper and lower graphs show the proteasome activity 1 h and 3 days after injection, respectively ($n = 8$). (b) Ubiquitinated proteins of the whole brain (3 days after injection). β-Actin is for the loading control. The graph indicates the densitometric analysis of ubiquitin/β-actin and monoubiquitin/β-actin band ($n = 8$). $^{*}p < 0.05$; $^{***}p < 0.001$.

 

## Results

### Successful administration of materials into CSF of medaka

Using a glass micropipette coupled to a Hamilton syringe, various toxins and drugs were successfully delivered to medaka via the CSF. To verify drug delivery into the CSF but not in the brain parenchyma, we injected a fluorescent dye as a marker. Soon after injection, fluorescence was visible in the CSF space. After removal of the skull and adjacent structures, the signal totally disappeared, indicating that the dye did not enter the brain parenchyma (Fig. 1b). This method of drug delivery was used for all of the following experiments.

### Reduced proteasome activity and increased ubiquitinated proteins in medaka treated with lactacystin

Proteasome activity was measured in the whole brain of normal, untreated medaka to determine baseline levels of proteasome activity (Fig. 2a) and compared with proteasome activity measured in medaka at different time-points following injection of the proteasome inhibitor lactacystin and the neurotoxin 6-OHDA. Each brain was intensively washed by PBS before the homogenization to avoid the carry-over of injected materials. The fluorescence signals increased linearly for the entire 60 min assay (data not shown). Addition of epoxomicin, a specific proteasome inhibitor, into the reaction buffer perfectly inhibited the fluorescence signals indicating this assay indeed reflected the proteasome activity. One hour after lactacystin injection, the proteasome activity in medaka brain was markedly decreased from baseline levels. 6-OHDA-treated medaka brain also showed mild reduction of proteasome activity. Three days after injection, the proteasome activity of lactacystin-treated and 6-OHDA-treated medaka brain became comparable to that of control brains (Fig. 2a).

Next, we compared the amount of ubiquitinated proteins in vehicle- and lactacystin-treated medaka using western blotting. Because medaka ubiquitin amino acid sequence is

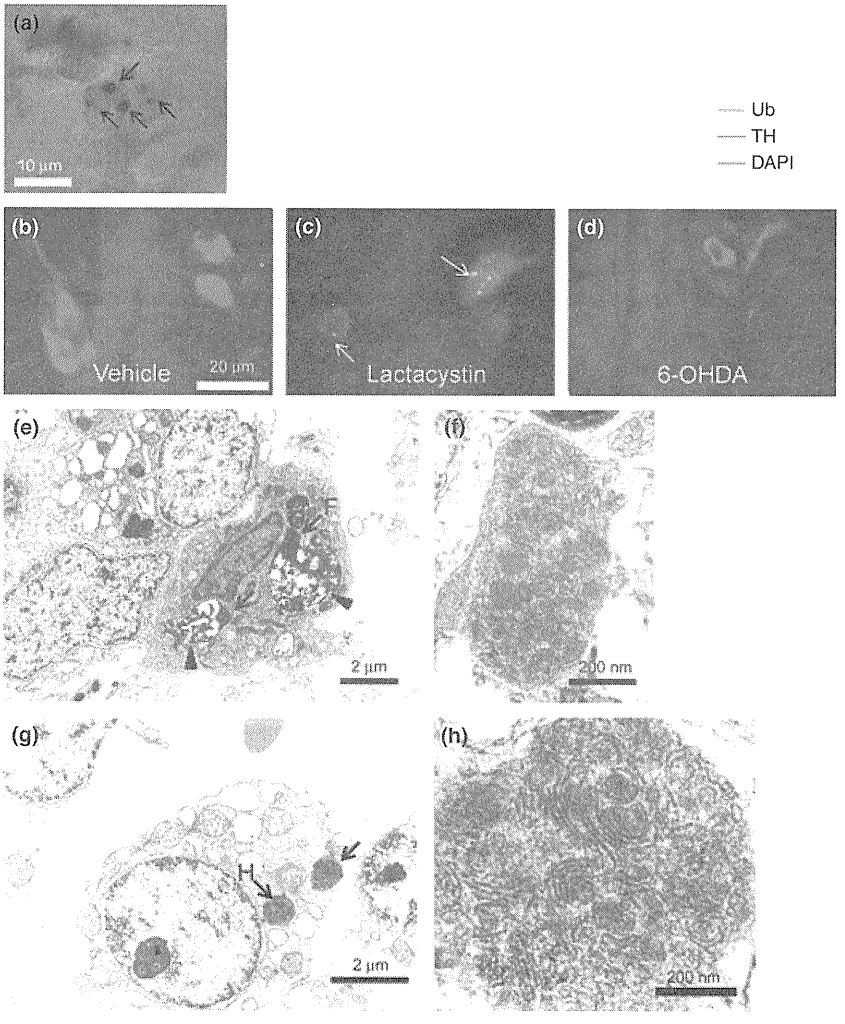


**Fig. 3** Images of inclusions of lactacystin-treated medaka brain. (a) Lactacystin-treated, 3,3′-diaminobenzidine (DAB) staining (anti-ubiquitin antibody). Arrows indicate ubiquitin-positive inclusions. (b–d) Immunofluorescence staining with anti-ubiquitin, anti-TH antibody and DAPI. (b) Vehicle-treated. (c) Lactacystin-treated. White arrows indicate ubiquitin, TH-double positive inclusions. (d) 6-OHDA-treated. (e–h) Electron microscopic photographs of lactacystin-treated medaka brain. Black arrows indicate the inclusions and arrow heads indicate the lysosome. (e, g) Some inclusions were seen adjacent to the nucleus. (f, h) Enlarged image of (e) and (g).

 

identical to human sequence, we used commercially available anti-ubiquitin antibody (rabbit polyclonal; Dako). Three days after lactacystin injection, high molecular weight ubiquitin-positive bands increased in lactacystin-treated medaka brains compared with levels in controls. 6-OHDA-treated medaka brain showed a more modest increase of ubiquitinated proteins. The amount of mono ubiquitin did not differ among the groups (Fig. 2b).

These findings suggest that injection of lactacystin inhibited proteasome activity in medaka brain, resulting in an increase in ubiquitinated proteins.

### Inclusion bodies seen in lactacystin-treated medaka

To test whether treatment with lactacystin resulted in an increase in inclusion bodies in medaka brain, we stained brain sections with an anti-ubiquitin antibody. Three days after injection of lactacystin, ubiquitin-positive cytoplasmic inclusions were seen in various regions of the brain (Fig. 3a). These inclusions were distributed throughout the brain, including the forebrain, optic tectum, diencephalon, hindbrain and spinal cord (data not shown). Some inclusions look like Lewy bodies, which are known to accompany PD (Fig. 3a). TH-positive neurons also contained inclusions

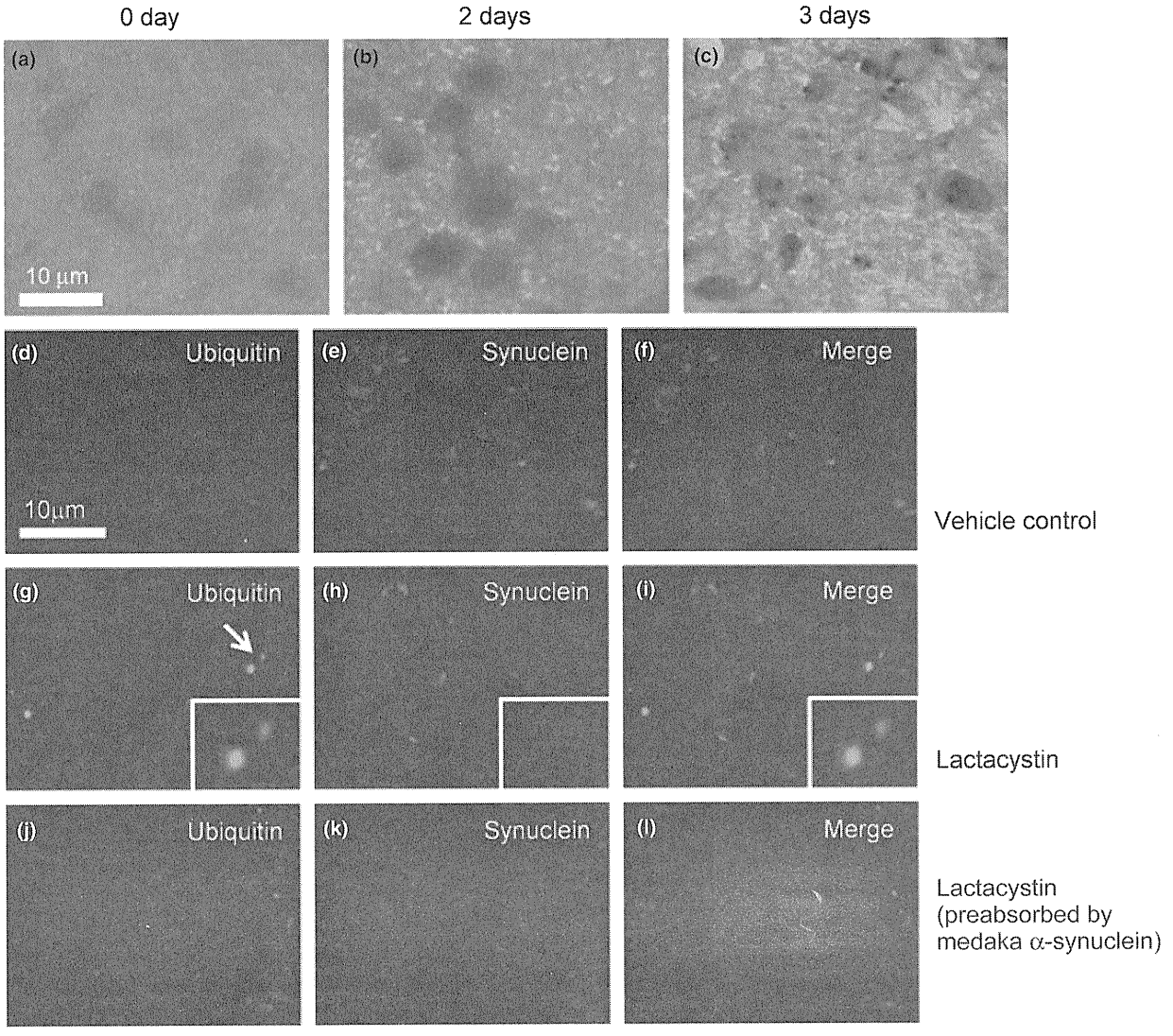


**Fig. 4** Time course of ubiquitin-positive inclusion formation in lactacystin-treated medaka brain (anti-ubiquitin antibody, (DAB) staining) (a–c), and anti-synuclein antibody staining 3 days after the injection (d–l). (a) 0 day, soon after the injection. (b) 2 days after the injection. The nucleus and cytoplasm showed diffuse signal enhancement. (c) 3 days after the injection. Multiple ubiquitin-positive inclusions appeared. (d–f) Control brain. (g–l) Lactacystin-treated brain. (d, g, j) Anti-ubiquitin antibody staining. (e, h) Anti-synuclein antibody staining. (k) Pre-absorption by recombinant medaka α-synuclein (10 μg/mL) disappeared the signals of synuclein antibody, indicating this antibody indeed recognized medaka α-synuclein. (f) Merged image of (d) and (e). (i) Merged image of (g) and (h). (l) Ubiquitin and synuclein did not colocalize. Merged image of (j) and (k). Each inset of (g), (h) and (i) is an enlarged image of inclusions (arrows).

 